國立臺灣大學電機資訊學院電信工程學研究所

碩士論文

Graduate Institute of Communication Engineering

College of Electrical Engineering and Computer Science

National Taiwan University

Master's Thesis

前列腺向膀胱內膨出之超音波影像分析

Intravesical Prostatic Protrusion Ultrasound Image Analysis

周敬庭

Ching-Ting Chou

指導教授：丁建均博士

Advisor: Jian-Jiun Ding, Ph.D.

中華民國 113 年 01 月

January, 2024

doi:10.6342/NTU202400113

國立臺灣大學碩士學位論文
口試委員會審定書
MASTER'S THESIS ACCEPTANCE CERTIFICATE
NATIONAL TAIWAN UNIVERSITY

前列腺向膀胱內膨出之超音波影像分析

Intravesical Prostatic Protrusion Ultrasound Image Analysis

本論文係__周敬庭____(姓名)_P09942A09__（學號）在國立臺灣大學電信工程學研究所完成之碩士學位論文，於民國_113_年_01_月_06_日承下列考試委員審查通過及口試及格，特此證明。

The undersigned, appointed by the Graduate Institute of Communication Engineering on_06_(date)_01_(month)_113_(year) have examined a Master's Thesis entitled above presented by_Ching-Ting Chou__(name)__P09942A09____ (student ID) candidate and hereby certify that it is worthy of acceptance.

口試委員 Oral examination committee:

丁建均　　　　　　　　　曾易聰

（指導教授 Advisor）

許文良　簡鳳村

所長 Director: 周錫增

誌謝

能夠順利地完成這篇論文要非常感謝老師的指導，在研究的過程中，總是能適時的點出盲點並給予建議。提供我很多實驗的方向跟建議，並且每次都可以在我無法理解時都能給予大量的解說，老師真的是我碩士求學最感謝的人。

另外也很感謝合作的張主任醫師他除了給我提供實驗的素材以外也提供很多醫療端的知識，並告知該實驗在臨床上的意義，讓我對自己的研究感到更有價值，並且常常抽出時間來跟我看實驗結果的問題並給我下一步的方向，今天的研究完全要感謝兩位學術跟醫界翹楚的幫助。

最後，希望我認識與認識我的每一個人身體健康、心想事成，此次的實驗能順利完成必須感謝非常多人在不同方面的協助。

doi:10.6342/NTU202400113

中文摘要

藉由電腦視覺以及醫療資訊兩個領域的結合，傳統超音波影像在醫療領域中很多都藉由人為判讀，但本次研究希望藉由電腦視覺的影像分析技術，提出一套可公式化的方法來處理超音波影像並提出判讀超音波影像的方法，研究主題主要針對膀胱及攝護腺的凹陷指數來判讀前列腺向膀胱內膨出的狀態，我們主要使用的識別方法包含:雜訊濾除、邊緣偵測、動態閥值、形態學、最短距離評估來做處理。並使用 PCA 距離測量及中心點垂直距離等方法來做量測標準。

我們藉由濾除雜訊，找尋相對位子，對膀胱輪廓的規則整理，閥值比較以及分割合併還有橢圓近似等方法，能夠推斷出膀胱超音波影像的凹陷病變指數(IPP)並藉由橢圓近似還原出膀胱原本該有的樣子。

關鍵字：膀胱凹陷、攝護腺病變特徵、前列腺向膀胱內膨出、超音波影像、醫療影像處理。

doi:10.6342/NTU202400113

Abstract

By combining computer vision and medical information, traditional ultrasound images in the medical field are often interpreted manually. However, in this study, we aim to propose a formulaic approach for processing ultrasound images and present a method for interpreting ultrasound images through computer vision techniques. The research focuses on the depression index of the bladder and prostate to assess the condition of the prostate protruding into the bladder. The identification methods used primarily include noise elimination, edge detection, dynamic threshold, morphology, and shortest distance evaluation. Additionally, we employ PCA distance measurement and vertical distance from the centroid as measurement standards.

Through the elimination of noise, determination of relative positions, regularization of bladder contours, threshold comparison, segmentation and merging, and elliptical approximation, we can infer the intravesical prostatic protrusion (IPP) of bladder ultrasound images. By utilizing elliptical approximation, we aim to reconstruct the original appearance of the bladder from the ultrasound images.

Keywords: Bladder indentation, features of prostatic lesions, Intravesical Prostatic Protrusion (IPP), ultrasound image analysis, medical image processing.

doi:10.6342/NTU202400113

Contents

口試委員會審定書 i

誌謝 ii

中文摘要 iii

Contents v

List of Figures vii

Chapter 1 Introduction 1

1.1 Motivation 1

1.2 Main Contribution 2

1.3 Organization 2

Chapter 2 Reviews of Computer vision image Process Algorithms 3

2.1 Filtering method 3

2.1.1 Mean Filter 4
2.1.2 Median Filter 4
2.1.3 Gaussian filter 5

2.2 Boundary Descriptors 5

2.3 Morphology 7

2.3.1 Erosion 7
2.3.2 Dilation 8
2.3.3 Opening 9
2.3.4 Closing 10

Chapter 3 Reviews of Biomedical Knowledge 12

3.1 Ultrasound 12

3.2 Biomedical Domain Concept 12

3.2.1 Biomedical Ultrasound Image 12
3.2.2 Bladder 13
3.2.3 Prostate 14

doi:10.6342/NTU202400113

3.2.3 Intravesical Prostatic Protrusion(IPP) 14
Chapter 4 Process Image Method 16
4.1 Introduction 16
4.2 Preprocess Image 18
4.2.1 Remove text data 19
4.2.2 Image Segmentation 19
4.2.3 Removing unnecessary label 20
4.3 Process Image 21
4.3.1 Noise Filtering 21
4.3.2 Chose Threshold 22
4.3.3 Remove Irrelevant Regions 25
4.3.4 Find Bladder Main Region 28
4.3.5 First Extension 29
4.3.6 Compare and expand of bladder 32
4.3.7 Find Final Bladder Position 37
4.3.8 Get Bladder Turning Point 38
4.3.9 Estimated Bladder Health Image 41
Chapter 5 Scoring Compare 45
5.1 Physician's marking calculation 45
5.2 Midpoint vertical distance 46
5.3 Ellipse PCA distance 48
5.4 Unit Conversion 51
5.5 Result Compare 52
5.6 Error attribution 54
Chapter 6 Experimental Results 58
Chapter 7 Conclusion 62
Reference 64

doi:10.6342/NTU202400113

List of Figures

Fig. 2 1 Gaussian function used for Gaussian filter.....5
Fig. 2 2 Boundary Descriptors Weight distribution diagram.....7
Fig. 2 3 Boundary Descriptors Forward execution diagram.....7
Fig. 2 4 Erosion Schematic Diagram.....8
Fig. 2 5 Dilation Schematic Diagram.....9
Fig. 2 6 Opening Schematic Diagram.....10
Fig. 2 7 Closing Schematic Diagram.....11
Fig. 3 1 The noise in ultrasound images.....13
Fig. 3 2 Intravesical Prostatic Protrusion.....15
Fig. 4 1 Flow Chart.....17
Fig. 4 2 Ultrasound images of the bladder and prostate.....18
Fig. 4 3 Ultrasound images after Preprocess.....21
Fig. 4 4 Examples of adaptive threshold result......24
Fig. 4 5 Examples of removing irrelevant regions in different thresholds. 27
Fig. 4 6 Examples of finding bladder main region.....29
Fig. 4 7 Examples of First Extension......32
Fig. 4 8 Examples of Extension......37
Fig. 4 9 Examples of Final Bladder Outline.....38
Fig. 4 10 Bladder Turning Point :.....40
Fig. 4 11 Ellipse.....42
Fig. 4 12 Examples of estimated bladder in healthy conditions......44
Fig. 5 1 Physician's marking calculation.....46
Fig. 5 2 Comparison of Actual Results in IPP......47
Fig. 5 3 PCA distance.....50
Fig. 5 4 Unit Conversion Image......51
Fig. 5 5 Error attribution Reason.....57
Fig. 6 1 Images result compare.....61

doi:10.6342/NTU202400113

Chapter 1
Introduction

1.1 Motivation

In urology, intravesical prostatic protrusion is a condition that often requires surgery, and the degree of prostatic depression is a key factor affecting a physician's decision regarding the necessity of surgery. However, there has been relatively little prior research in the field of image analysis, particularly in the automated interpretation of ultrasound images related to the prostate. Most studies related to the bladder involve clinical interpretation, invasive treatments for prostate issues, and subsequent medical research on the effectiveness of these treatments.

Interpreting unclear ultrasound images of the bladder and analyzing intravesical protrusion are essential processes. Most manual interpretation methods can vary among physicians, and sometimes, images can be challenging to interpret due to ultrasound noise interference. Therefore, we plan to combine computer vision techniques with medical expertise to develop an automated method for discerning intravesical prostatic protrusion in ultrasound images.

In clinical practice, overseas patients often require the assistance of family physicians to determine whether a referral to a specialist is necessary. However, family physicians may lack relevant background knowledge when interpreting bladder ultrasound images. Thus, we propose an automated interpretation process that can be beneficial for family physicians in foreign countries to analyze whether patients need

doi:10.6342/NTU202400113

specialized care. We hope that our research can provide a comprehensive method for processing medical ultrasound images, which can also be applied to ultrasound images of other body parts.

1.2 Main Contribution

Our main contributions are summarized as follows.

1. We propose an Ultrasonography processing algorithm in which we successfully Identify features in ultrasound images.
2. We propose an algorithm to calculate the Interpretation of Intravesical Prostatic Protrusion. Interpretation problem.
3. We have established a standardized method to represent bladder concavity, replacing the previously imprecise manual measurements.
4. With our method doctor can quickly label the positions of the bladder and bladder deformation to facilitate further disease analysis or other related disease analysis.

1.3 Organization

This thesis is organized as follows: In Chapter 1: We Introduce research contributions and motivations. In Chapter 2: We present an overview of the Classic computer vision processing algorithm. In Chapter 3: We provided a brief overview of some medical background knowledge that will be used. In Chapter 4: We introduce the step and algorithm that we used to propose the Image. In Chapter 5: We have introduced the medical measurement method and the PCA measurement for comparing the results between the label image and our result. In Chapter 6, We showcase the

doi:10.6342/NTU202400113

outcomes of our processing and present comparative images with the original annotations. Chapter 7, We conclude our algorithm and compare the advantages and disadvantages of our method, as well as the feedback from the medical community regarding our approach.

Chapter 2
Reviews of Computer vision image Process Algorithms

Although there are many AI algorithms, such as CNN (Convolutional Neural Networks) and RNN (Recurrent Neural Networks), available for image processing. The challenge we need to process today is that relevant ultrasound images always have been interpreted based on the experience of physicians, with limited label data. Therefore, we need to rely on traditional computer vision processing methods to convert the medical domain's experiential knowledge into algorithms for processing these images. In this context, we will also provide an introduction to the computer vision algorithms that we use or are relevant.

By utilizing these traditional methods, we can explicitly help physicians understand our processing steps. In contrast to machine learning, this approach allows for a more transparent comparison of cognitive differences with users. It also enables the algorithm to be applied to other ultrasound image-processing tasks beyond the scope of this experiment.

2.1 Filtering method

Filters Introduction:

doi:10.6342/NTU202400113

General Filters:

General filters can be applied in various signal processing domains, including audio, image, video, digital signal processing, and more.

General filters can come in different types, including low-pass, high-pass, band-pass, and band-stop, used to filter, enhance, or suppress signal components within specific frequency ranges.

Image Filters:

Image filters are a specialized type of filter designed specifically for the field of digital image processing.

These filters are primarily used to process and enhance digital images to improve image quality, reduce noise, enhance details, or detect specific features.

Ultrasound images often contain a lot of noise, including speckle noise. So when processing ultrasound images, it is essential to appropriately filter out this noise. However, excessive filtering can lead to the removal of essential features. Therefore, it is crucial to make the right choices when selecting filters and their parameters.

So we will provide a basic introduction to the image filters we use and compare them in our study.

2.1.1 Mean Filter

Mean filter [1][2] is a smoothing filtering method commonly used to reduce high-frequency noise in images. It calculates the average of the pixels in the neighborhood of each pixel and replaces the pixel's value with this average.

2.1.2 Median Filter

Median filter [1] is a non-linear filtering method often used to remove

doi:10.6342/NTU202400113

salt-and-pepper noise and other types of noise. It replaces each pixel with the median value of its neighborhood pixels.

2.1.3 Gaussian filter

Gaussian filter[3][4] uses a Gaussian function [5] to weight the pixels in its neighborhood, achieving a smoothing effect. This method is commonly used to reduce high-frequency noise. Its pulse function's weighting is modeled to follow a normal distribution near the origin.

In simple terms, a Gaussian filter is used to perform a weighted average on the entire image. It applies a Gaussian function to combine the central pixel with its neighboring pixels, creating a new pixel matrix. This method is commonly referred to as convolution.

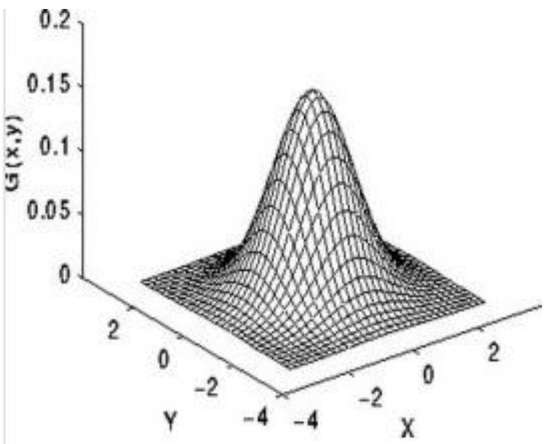

Fig. 2 1 Gaussian function used for Gaussian filter [6]

2.2 Boundary Descriptors

Boundary Descriptors [7] is a method used to describe the contours of objects, often combined with concepts like curvature and bending energy. This approach is primarily employed for irregular objects, aiming to capture and describe the edge

doi:10.6342/NTU202400113

contours of an object. Unlike other shape descriptors, the primary goal of Boundary Descriptors is to quickly and effectively identify the outline of an object, rather than analyzing other features such as centroid, area, texture, shape, or relative orientation.

The advantage of this method is its ability to rapidly locate the object's outline through fast matrix operations. It is suitable for applications that require quick detection and description of object contours, such as object detection, object recognition, and image segmentation. Especially when dealing with objects with irregular shapes, Boundary Descriptors can effectively assist in extracting and representing their contour information, laying the foundation for subsequent edge analysis.

The method begins with the center point of the original 3x3 grid as the initial point. It reallocates new weights to determine the next direction to move based on the previous point's position. With each step, the weight distribution in the 3x3 grid of possible directions changes, and the algorithm keeps changing direction until it returns to the starting point. The approach involves using the line formed by connecting the previous point to the current point as the direction to move, and it uses this line as an arrow to generate numbers from 1 to 8 in a clockwise manner for the next step. You have added some special conditions in your experiment to allow revisiting points, which is particularly useful in ultrasound images with many concave features. Thanks to the ever-changing weight distribution for the next direction, the algorithm can navigate successfully and avoid getting stuck in an infinite loop.

doi:10.6342/NTU202400113

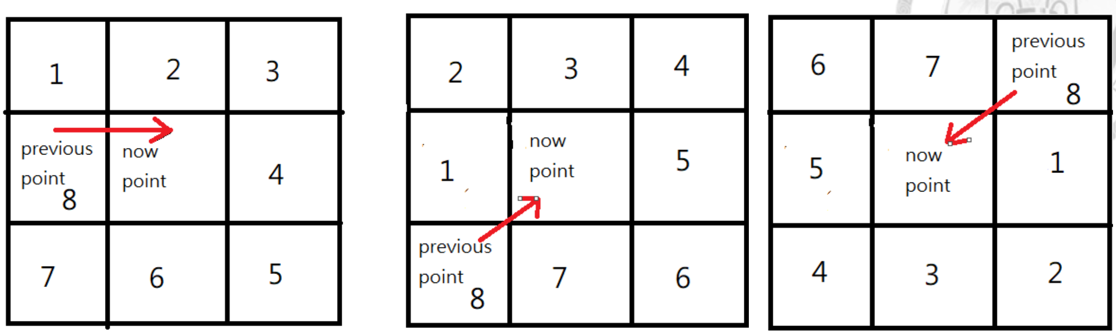

Fig. 2 2 Boundary Descriptors Weight distribution diagram

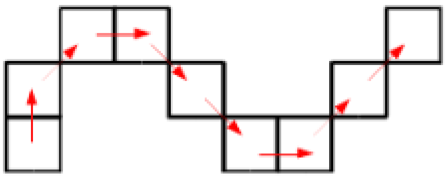

Fig. 2 3 Boundary Descriptors Forward execution diagram [7]

2.3 Morphology

Morphology [8] is a technique used in image processing and analysis. It involves operations on the relationships between pixels to adjust and analyze the shapes and structures within an image. Common morphology operations include erosion, dilation, opening, and closing. These methods can alter the shape, size, and structure of objects in an image. Morphology is often used in applications like image segmentation, object detection, texture analysis, shape feature extraction, hole filling, and connectivity analysis.

2.3.1 Erosion

Erosion [9] [12][13] is a morphological operation used to shrink or reduce the edges of objects in an image. It is expressed by (1) in order.

doi:10.6342/NTU202400113

$$E(A,B) = A\theta(-B) = \bigcap_{b\in -B} A + b \qquad (1)$$

where A is original image elements, B is structuring elements

Take the intersection of each point in Figure A after moving it up, down, left, and right. Shrink or reduce the edges of objects.

It typically involves a small kernel (also known as a structuring element) that slides over the image and is used to "erode" the edges of objects, making them smaller.

Main uses: Separating objects that are close to each other, decreasing an object's size, and growing the holes enclosed by a single area.

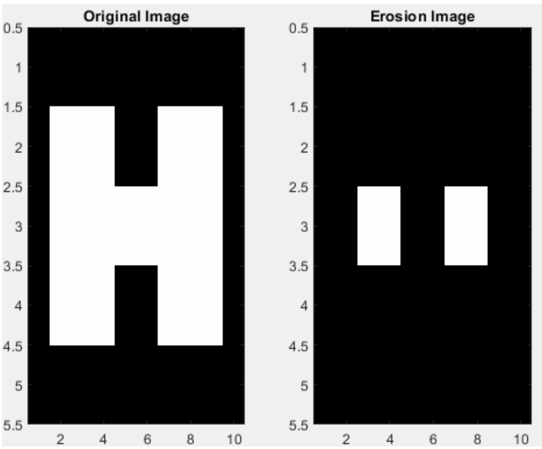

Fig. 2 4 Erosion Schematic diagram

2.3.2 Dilation

Dilation [12][13] is a morphological operation used to expand or increase the edges of objects in an image. It is expressed by (2) in order.

$$D(A,B) = A \oplus B = \bigcup_{b\in B} A + b \qquad (2)$$

where A is the original image elements, and B is the structuring elements.

doi:10.6342/NTU202400113

Take the union of each point in Figure A after moving it up, down, left, and right.

Similar to erosion, it also uses a structuring element, but it expands the edges of objects.

Main uses: Connecting disjointed objects, increasing the size of objects, and shrinking the holes enclosed by a single area.

Fig. 2 5 Dilation Schematic diagram

2.3.3 Opening

Opening [10][11] [12][13] is a combination of erosion and dilation operations, first performing erosion and then dilation. It is expressed by (3) in order.

$$A \circ \mathrm{B} = (A \ \ \theta \ \ B) \oplus B \tag{3}$$

where A is original image elements, B is structuring elements

It is typically used to remove small noisy objects while preserving the shape of the main objects.

Main uses: Separating closely located objects, smoothing object contours and

doi:10.6342/NTU202400113

fractures, narrow isthmuses, eliminating the thin protrusions.

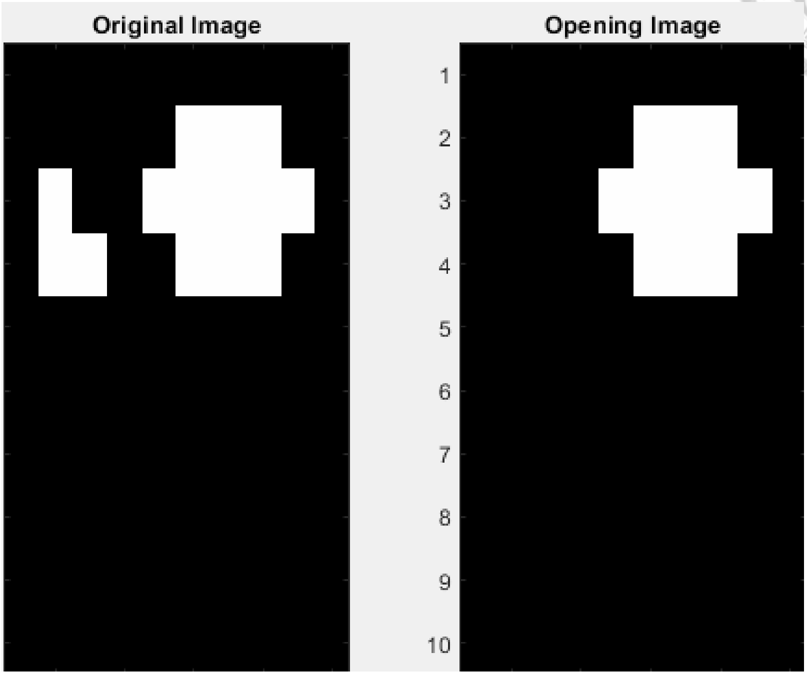

Fig. 2 6 Opening Schematic diagram

2.3.4 Closing

Closing[10][11] [12][13] is a combination of dilation and erosion operations, first performing dilation and then erosion. It is expressed by (4) in order.

$$A \bullet B = (A \oplus B)\theta B \qquad (4)$$

where A is original image elements, B is structuring elements

It is typically used to close small gaps between objects or connect disjointed objects.

Main uses: Connecting separated objects, filling gaps, smoothing object contours and fractures, removing small holes.

doi:10.6342/NTU202400113

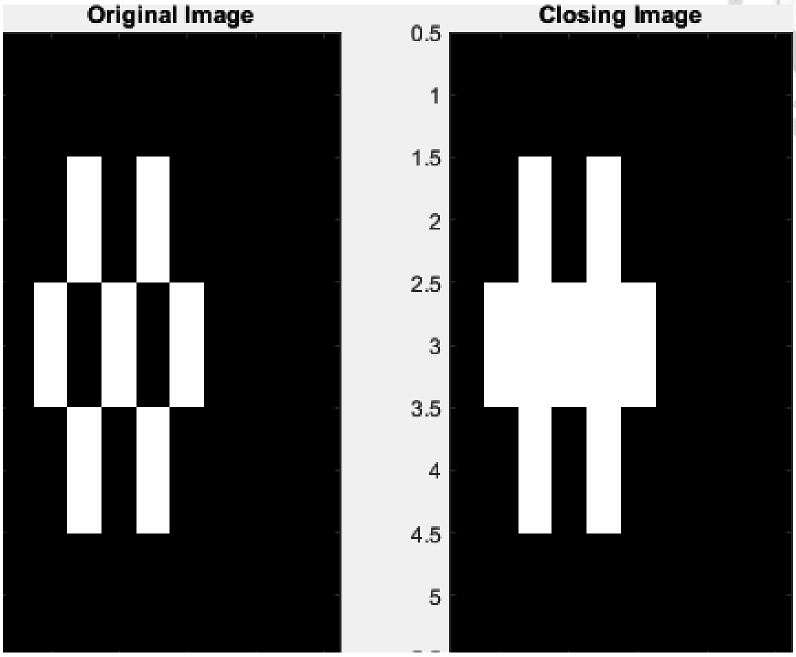

Fig. 2 7 Closing Schematic diagram

doi:10.6342/NTU202400113

Chapter 3
Reviews of Biomedical Knowledge

3.1 Ultrasound

Ultrasound [14] is a type of mechanical wave that originated from sonar technology. Its principle involves using frequencies higher than what can be heard by the human ear, typically ranging from approximately 2 MHz to 10 MHz. Ultrasonic waves have the characteristics of high frequency, short wavelength, and linear propagation, making them prone to refraction and reflection. This makes ultrasound a valuable tool for investigating objects that are not visible with ordinary light. The method involves emitting high-frequency ultrasound pulses and then capturing their echoes. The delay in the return of echoes and their intensity provides information about the internal structure of objects. Ultrasonic imaging is the process of presenting this information in the form of images. Currently, ultrasound finds common applications in medicine and industry, primarily for imaging, detection, and measurement.

3.2 Biomedical Domain Concept

3.2.1 Biomedical Ultrasound Image

Ultrasound imaging [15] [16] is a process that involves emitting high-frequency sound wave pulses and capturing their reflected echoes to create images. These sound waves produce echoes as they interact with different tissues and structures, and a computer analyzes these echoes and transforms them into images displayed on a monitor. The advantages of ultrasound imaging include its non-ionizing nature,

doi:10.6342/NTU202400113

allowing observation of organ motion and blood flow, making it a non-invasive imaging technique. Additionally, ultrasound equipment is relatively cost-effective compared to some other imaging technologies, and it can provide imaging when light cannot penetrate.

However, ultrasound imaging has its drawbacks. When ultrasound needs to penetrate deep tissues, its imaging effectiveness is reduced, making it less suitable for deep organ imaging. Furthermore, when sound waves reflect multiple times within tissues, it can lead to the appearance of artifacts or echoes and may be subject to interference, resulting in the presence of various forms of noise. Typically, ultrasound imaging exhibits pronounced blurring, particularly when sound waves interact at different tissue interfaces. The issue of increased noise and image blurring is a significant challenge we aim to address in our experiment.

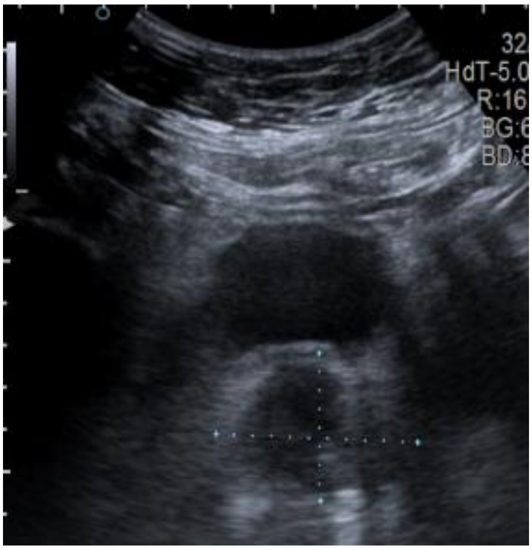

Fig. 3 1 The noise in ultrasound images

3.2.2 Bladder

The bladder [17] is an important organ in the human body, primarily located in the

doi:10.6342/NTU202400113

pelvic area, in front of the lower abdomen. It is a pouch-like organ that, under normal conditions, takes on a shape resembling an ellipse in ultrasound imaging due to pressure. The bladder serves as a storage and excretion organ for urine. At the top of the bladder, there is an area known as the bladder neck, which leads to the urethra. When the muscles of the bladder receive neural signals from the brain, they contract to expel urine into the urethra, allowing the process of urination to occur.

3.2.3 Prostate

The prostate [18] is an important organ in the male reproductive system, located within the pelvic area. It is about the size of a cherry and surrounds the urethra, closely adjacent to the base of the bladder. This organ plays a crucial role in the male reproductive and urinary systems, aiding in the protection and nourishment of sperm to enhance their motility during ejaculation.

3.2.3 Intravesical Prostatic Protrusion(IPP)

Intravesical Prostatic Protrusion [19], or simply IPP, refers to a condition in which a portion of the prostate extends into the bladder. The prostate is typically located beneath the bladder and surrounds the urethra. When prostate tissue undergoes inward growth or enlargement, it may exert pressure on the bladder, causing a portion of the prostate tissue to intrude into the bladder cavity from its normal position. This can lead to symptoms such as difficulty urinating, increased urinary frequency, and urgency. In cases of mild IPP, special treatment may not be required. However, severe symptoms may necessitate surgical intervention. The diagnosis is typically conducted using ultrasound imaging, which is the focus of our current endeavor to automate the symptom assessment.

doi:10.6342/NTU202400113

According to the literature, an IPP (Intravesical Prostatic Protrusion) typically exceeding 5.5 millimeters is known to result in urination difficulties[20]. Therefore, in the subsequent sections of our paper, we will conduct further assessments based on this phenomenon.

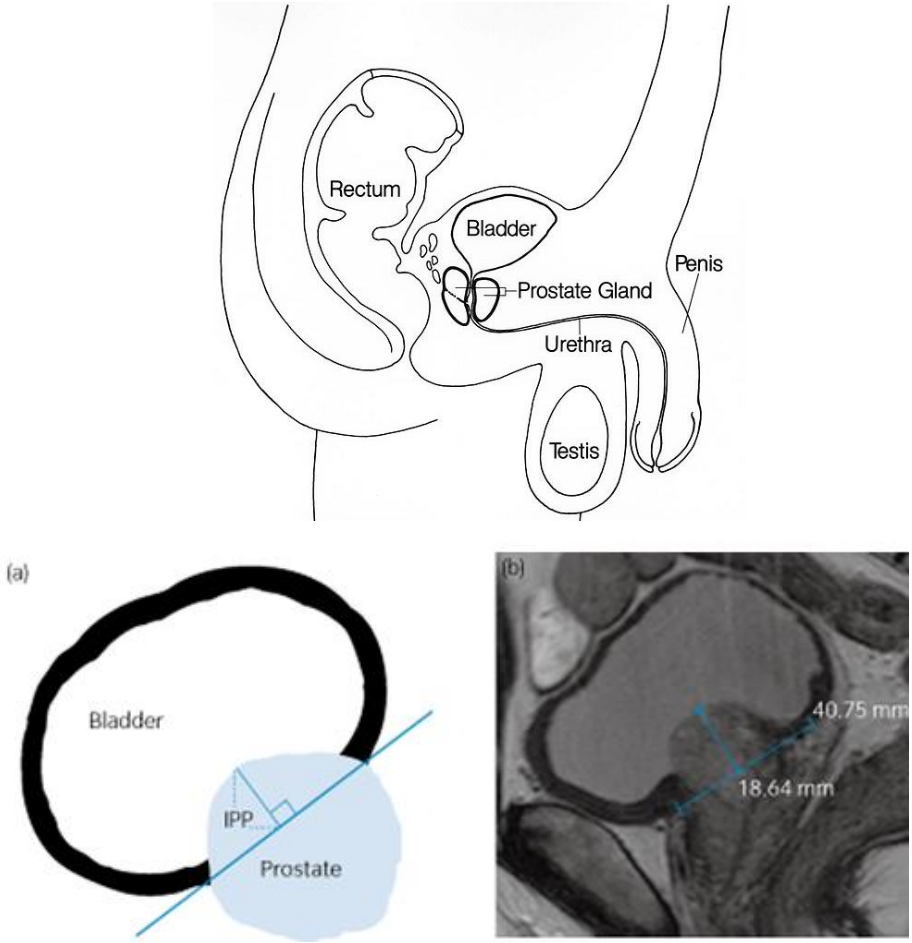

Fig. 3 2 Intravesical Prostatic Protrusion [21][22]

doi:10.6342/NTU202400113

Chapter 4
Process Image Method

4.1 Introduction

Our collaborative experiment is with the urology department of a certain hospital, focusing on the processing of ultrasound images of the bladder and prostate. The primary objective is to determine the degree of bladder concavity from these images to infer the condition of the prostate. We've achieved this through multiple interviews and discussions with the physicians to understand their clinical approach to interpreting ultrasound images. Using computer vision and relevant literature, we're gradually working towards automating the interpretation method.

The main challenges we're addressing in this research include handling noise in ultrasound images, dealing with text interference in the original images, identifying the complete bladder and prostate, evaluating bladder concavity, estimating the healthy appearance of the bladder before any pathological changes, achieving assessment with limited labeled data and medical expertise introduction, and ultimately, and introducing our processing method and steps to medical personnel and obtaining their approval.

In the following sections, I will introduce our approach for this study, and many details on computer vision techniques and methods have already been discussed in Chapter 2, and Biomedical knowledge in Chapter 3

doi:10.6342/NTU202400113

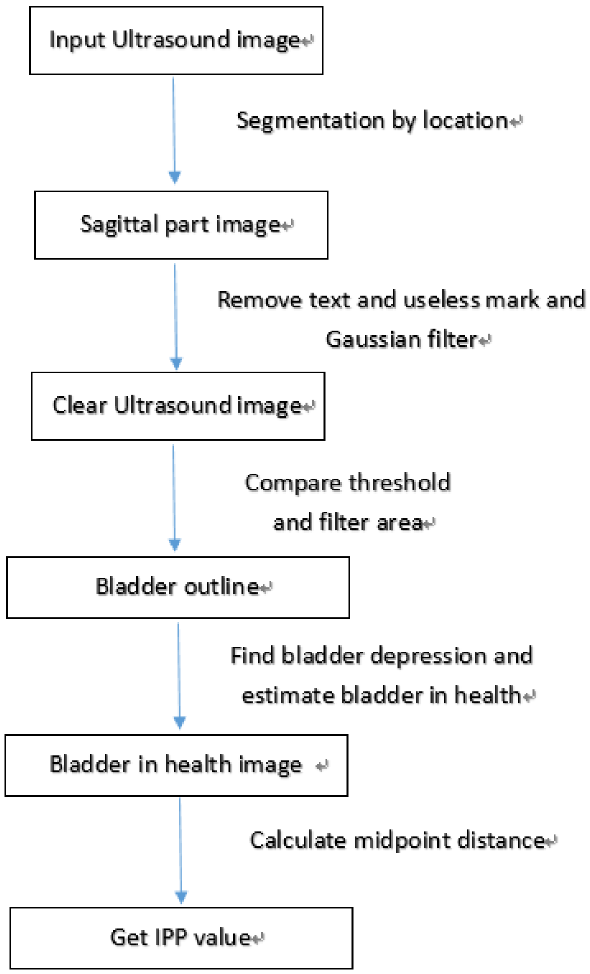

Fig. 4 1 Flow Chart

doi:10.6342/NTU202400113

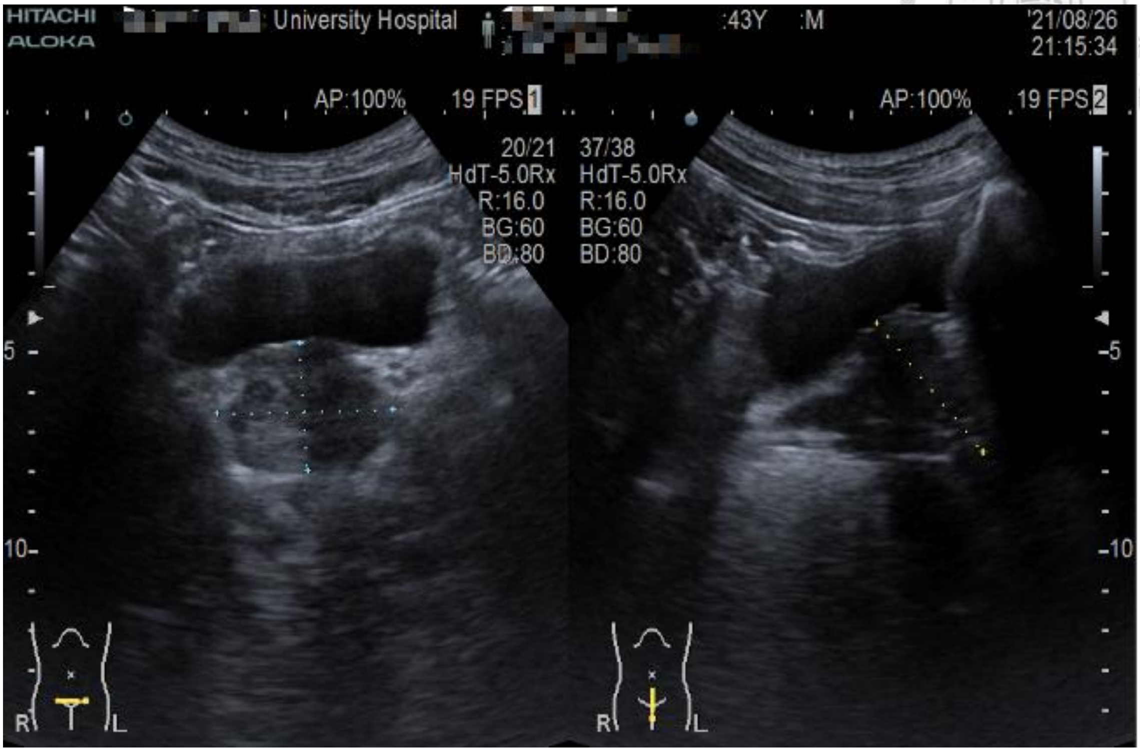

Fig. 4 2 Ultrasound images of the bladder and prostate

4.2 Preprocess Image

Fig. 4.1 (above) is one of the images we need to process. Before starting the formal computer vision processing, we can identify several issues from this image. The first issue is that the image can be divided into the left half and the right half. The left half is the 'Transverse view,' and the right half is the 'Sagittal view.' In discussions with the collaborating physician, we were informed that measuring Intravesical Prostatic Protrusion (IPP) is done using the Sagittal view. Therefore, we need to perform image segmentation to extract the part we need for processing.

The second issue is that we can see a lot of non-image text on the image, including English names, hospital record numbers, and ages (I have already obscured them with a mosaic in the paper). While this text does not contain precise personal privacy

doi:10.6342/NTU202400113

information, for safety reasons and to reduce their impact on our image interpretation, we also need to remove them.

The third issue is that the image contains many unnecessary borders and annotations, which, similar to text, might slightly affect image interpretation. So, we also need to eliminate these unnecessary borders and annotation lines before we can start the formal image processing. Below, I will explain how I preprocess these issues step by step.

4.2.1 Remove text data

I removed the text by specifying a fixed position and color. After careful observation of the pixels and positions of each text element, I found that the main color combinations were (190, 190, 190), (255, 227, 80), and (134, 220, 255). Of course, there were other colors as well, but I initially targeted the top-left diagonal, top-right diagonal, and left, and right sides to eliminate these annotations. Once I removed these points, I used the average color of the four neighboring pixels to fill the gaps. If two or more points in a row were removed, I extended the region to obtain the average color of the surrounding area to fill in the missing central area. Using this method, we obtained an image without any text interference.

4.2.2 Image Segmentation

Just like the previous introduction, the medical images that will be used in the clinical setting are the Sagittal view on the right side. To ensure precise assessment, we need to crop the images. First, we identify the midpoint of the image and split it into

doi:10.6342/NTU202400113

two separate images. Then, we perform some processing. This is primarily because ultrasound images are only located in the central portion of the image, and there may be some borders in the peripheral areas that could affect image interpretation. Therefore, we remove these areas to retain only the central region in our processed images, which is the main area we want to analyze. We have removed unnecessary regions from most of the images as a part of our preprocessing.

4.2.3 Removing unnecessary label

This part is similar to removing text, but it mainly focuses on removing certain annotations, including centimeter markers on the left and right sides (which will be used for distance calculations later, but we need to remove them for now). It also includes markings in the middle blue and yellow areas. These are annotations made by specialists to indicate the position of the bladder. However, in this context, they will only interfere with our image analysis. The removal method primarily targets pixels with RGB values indicating yellow. Additionally, we need to remove the bottom marker that shows the direction of the ultrasound scan. These areas are treated similarly to text removal, focusing on specific positions and RGB pixel values. The filling method after removal is the same.

doi:10.6342/NTU202400113

Fig. 4 3 Ultrasound images after Preprocess

4.3 Process Image

4.3.1 Noise Filtering

Because, as mentioned earlier, ultrasound images contain a lot of noise, we aim to minimize noise interference in image analysis to better detect positions. However, we also have concerns that excessive smoothing might filter out the objects we want to detect. Therefore, after considering several common filters mentioned above, we decided to use a Gaussian filter. Here is the kernel formula we use

$$\text{kernal} = \frac{1}{c} * e^{-\pi * \sigma * (x^2 + y^2)} \tag{5}$$

We use the kernel function for the Gaussian filter above. After setting the values of

doi:10.6342/NTU202400113

'c = 1' and 'σ = 10,' I convolution the kernel with the original image to perform noise reduction.

4.3.2 Chose Threshold

In this context, we need to choose a threshold to convert the image into black and white to identify the shape of the image. Initially, we used a fixed threshold value, but we realized that ultrasonic images vary in brightness, and even after filtering, some noise is still present. Therefore, we couldn't rely on a fixed value to find a general pattern. As a result, we later considered using an adaptive threshold.

First, we used a method similar to Gaussian filtering to obtain a smooth mask, which serves as the threshold. Then, we multiplied it by a coefficient for further filtering. Below are the coefficients and the formula we used.

$$\mathrm{smooth}[n] = \frac{e^{-\pi*\tau*n^2}}{\sum_{n'} e^{-\pi*\tau*n'^2}} \quad , -\mathrm{L} \le \mathrm{n}' \le \mathrm{L} \ , -\mathrm{L} \le \mathrm{n} \le \mathrm{L} \ , \tau = \frac{1}{L^2} \ ,$$

$$L = \frac{\min(\mathrm{Row}, \mathrm{Col})}{10} \tag{6}$$

We take the previously mentioned smooth filter and perform two convolutions with the original image to obtain a threshold. We apply different thresholds to filter the original image, resulting in different black-and-white binary images. Subsequently, we use 'complement' to invert the black and white areas, This process yields the example results shown in the image below.

doi:10.6342/NTU202400113

(a)

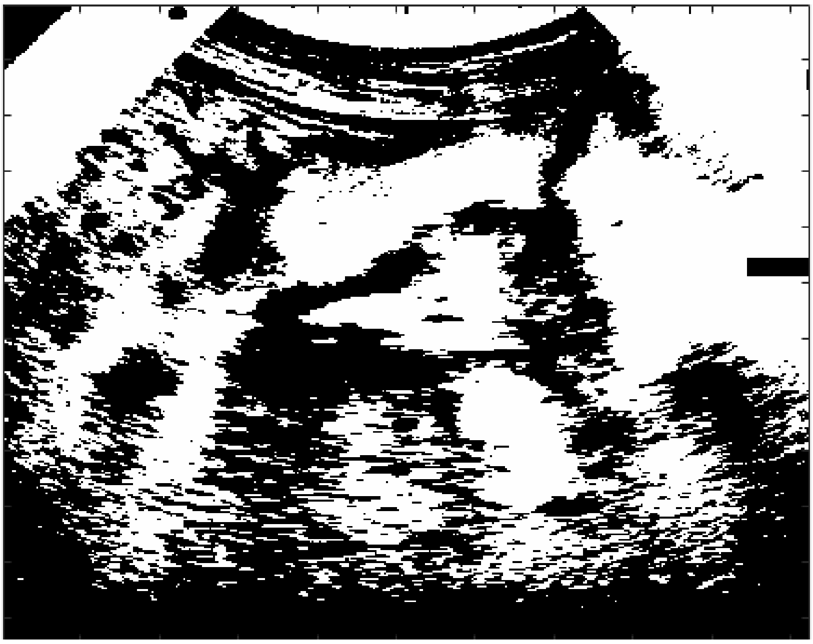

(b)

doi:10.6342/NTU202400113

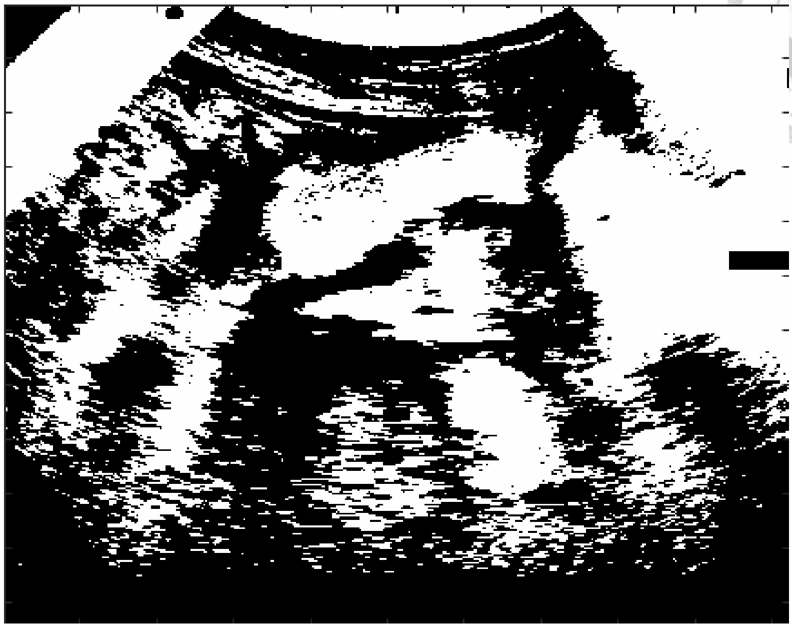

(c)

(d)

Fig. 4 4 Examples of adaptive threshold result.(a): Threshold = 1* Smooth. (b): Threshold = 0.9* Smooth. (c): Threshold = 0.8* Smooth.(d): Threshold = 0.6* Smooth.

doi:10.6342/NTU202400113

4.3.3 Remove Irrelevant Regions

From the results above, we can see the images at the imcomplement results of 0.6smooth, 0.8smooth, 0.9smooth, and 1.0smooth. However, we can observe that with lower smoothing values, fewer regions are retained. Even in the context of 0.6 ratio smoothing, there are still many small regions or other unrelated areas present. These areas can affect our interpretation. Therefore, we initially apply some basic filtering to these small blocks.

First, for small areas, we set a criterion to exclude any region with an area less than (length * width) / 100. Then, we proceed to filter out areas that are too far from the center of the image. We consulted with a physician, and the physician indicated that all IPP images are essentially located at the center of the image. Therefore, we can confidently filter out areas near the edges. To avoid excessive filtering, we set the condition that an area is only excluded when the center of that area is higher than length * 1/4 or lower than length * 3/4 or when it is to the left of width * 1/4 or to the right of width * 3/4. Below are example results of filtering for each of the thresholds.

doi:10.6342/NTU202400113

(a)

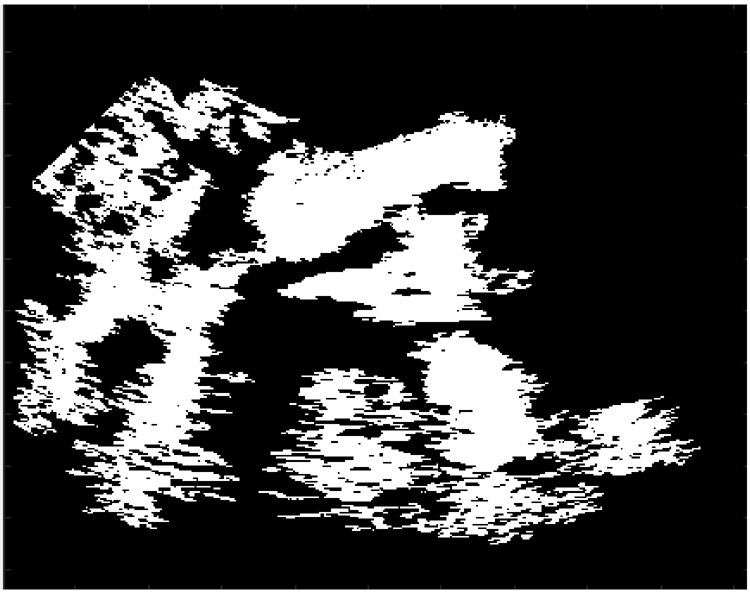

(b)

doi:10.6342/NTU202400113

(c)

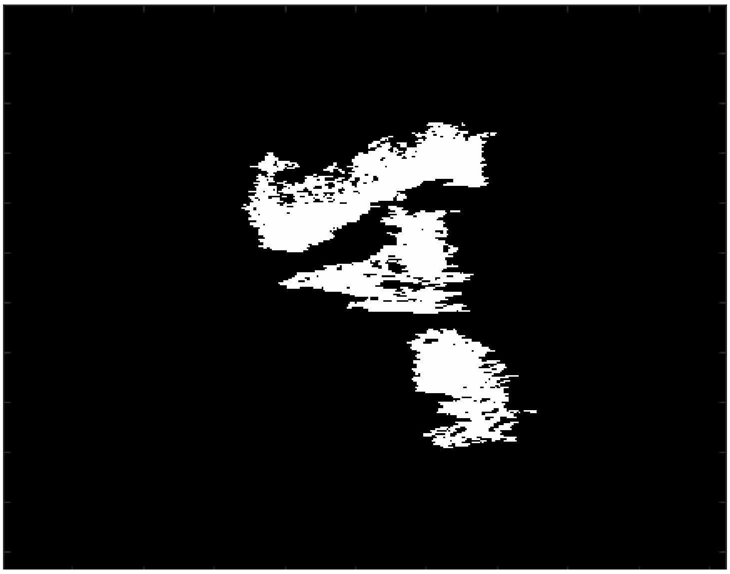

(d)

Fig. 4 5 Examples of removing irrelevant regions in different thresholds.(a): Threshold = 1* Smooth. (b): Threshold = 0.9* Smooth.(c): Threshold = 0.8* Smooth. (d): Threshold = 0.6* Smooth.

doi:10.6342/NTU202400113

4.3.4 Find Bladder Main Region

Based on the steps above, we found that the lowest smoothing coefficient scaling factor I used was only able to capture down to 0.6. This was because, during experiments, I observed that when the scaling factor was set lower than 0.6, some images, especially those where the bladder features were less distinct, resulted in parts of the bladder being filtered out. Therefore, I decided to set the minimum scaling factor to 0.6. Through all our annotations and test images, we discovered that, regardless of the chosen scaling factor, there was always a portion of the bladder within this range, with some areas completely black. While not all regions inside the bladder might be filtered by the threshold, we still needed to identify areas that could potentially be part of the bladder. Locating the bladder is a crucial step for us, and without identifying the main bladder region, we wouldn't be able to proceed with the next steps.

After going through the previous steps, we were able to obtain the approximate location of the bladder at a scaling factor of 0.6. However, there could still be additional large regions that, based on the original image interpretation, might be the prostate or simply meaningless empty areas. This is where our next step comes into focus: accurately identifying the bladder's position, essentially distinguishing which area is the bladder. We used two criteria for this determination: area and relative position. We scanned the image from top to bottom, and the first region we encountered with the highest central point and the largest area was considered the bladder. If larger areas were encountered further down, they were not considered as part of the bladder.

doi:10.6342/NTU202400113

Fig. 4 6 Examples of finding bladder main region

4.3.5 First Extension

After going through the above steps, we obtained the most basic outline of the bladder's location. However, there is still a significant difference from the expected appearance of the bladder. Therefore, we need to gradually expand the bladder to give it the desired contour. We will go through three main expansion steps, and this is our first expansion step. The primary method is to utilize the bladder position obtained through the previously mentioned method. Next, we compare it with the 0.9 * threshold image.

First, we apply 50 iterations of closing to the bladder's small region obtained from the 0.6 * threshold image. Afterward, we perform 15 iterations of opening on the 0.9 * threshold image. We then perform region segmentation using Bwlabel. Next, we take the regions and combine them with the results of closing from the 0.6 * threshold image for the same regions. In other words, if there is an intersection between the opening results from the 0.9 * threshold image and the closing results from the 0.6 * threshold image, we directly include that region in the 0.6 * threshold image for region expansion.

Here, we will explain in detail why we follow this approach. First, the reason for

doi:10.6342/NTU202400113

performing 15 iterations of opening on the 0.9 * threshold image is that the final expansion mainly focuses on the 0.9 * threshold case. Therefore, we need to disconnect each region through extensive opening because small connections are often due to unnecessary region linkages. Using the principles of opening, we separate these areas. The choice of 15 iterations is based on testing and finding a suitable balance.

As for performing closing on the 0.6 * threshold image, we initially identified the basic outline of the bladder, but there may be various fragmented conditions. Therefore, we use a larger number of openings to try to complement them as much as possible. Afterward, by performing a union expansion on the common areas between the two, we can obtain a union region basic bladder outline in the first step. It's worth mentioning that we focus on the segmentation of regions in the opening step. We only include an area if it overlaps with the closing regions, so sometimes it may be smaller than the closing image and possibly even smaller than the bladder obtained in the previous step. Below is a schematic diagram of one of our cases.

(a)

doi:10.6342/NTU202400113

(b)

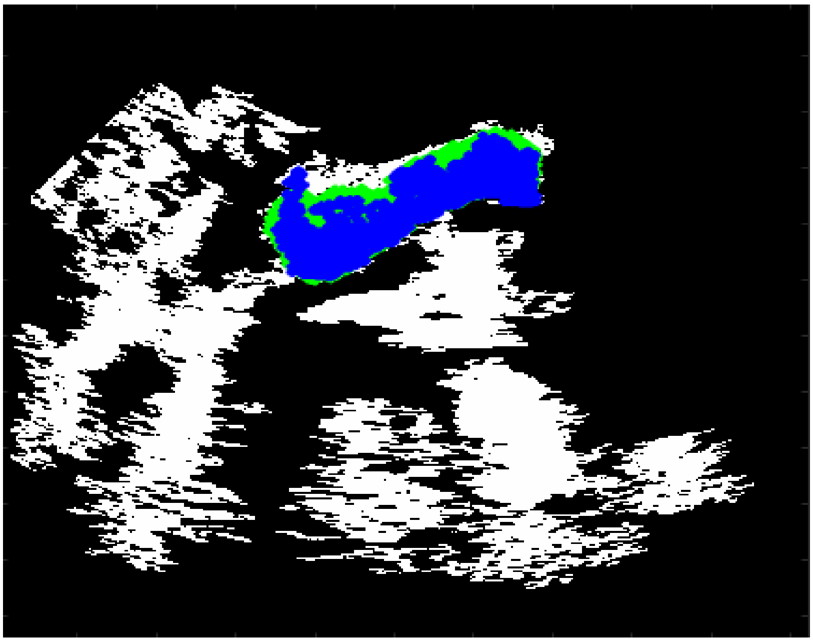

(c)

doi:10.6342/NTU202400113

Fig. 4 7 Examples of First Extension.(a): opening 0.9*Threshold by 15 times. (b): closing bladder main region 50 times. (c): the white region is 0.9*Threshold the blue region is the bladder main region and the green region is our expanded region.

4.3.6 Compare and expand of bladder

Using the method described above, we started with a scaling factor of 0.6 and removed unimportant areas, allowing us to identify a small portion of the main bladder region. After the first stage of expansion, the bladder expansion profile of the first stage was obtained. Subsequently, we want to gradually expand from this small area outward to find the contour of the main bladder region. We will undergo a total of three expansion stages. Here is the second step. Our approach involved using threshold images with different scaling factors for this expansion process. This approach was based on the understanding that, even though the bladder is the primary area with a relatively large and darker ultrasound imaging region, it doesn't mean that the entire bladder area's ultrasound image contour can be identified in the experiments. This is because there may be less distinct ultrasound imaging regions at the boundaries or certain points within the bladder region. Our method involved repeatedly expanding to find a more complete contour of this area by using different scaling factors for thresholding. We primarily utilized scaling factors of 0.6, 0.8, and 0.9 for this expansion and filtering process. In total, we underwent three rounds of expansion in this step, and after each expansion, we compared the results with images using higher coefficient thresholds before continuing the expansion.

doi:10.6342/NTU202400113

The following step-by-step instructions detail our expansion method. First, we utilize the bladder positions we obtained previously. Next, we compare the 0.6 times the threshold image. We use an Exclusive OR operation from white image blocks below 0.6 times the threshold to subtract the first step expended image. Then, we perform block segmentation using BWlabel on these blocks. Subsequently, we apply one closing operation, followed by three opening operations. Afterward, we perform BWlabel once more for block segmentation. These processed blocks are collectively referred to as "add regions."

Next, we scan each "add region" and exclude it if its size exceeds 1.5 times the original first step expended image area or if the area of the add region is too large, exceeding approximately 1000 pixels (i.e., (image length * image width) / 300) and if the center point of the added region is to the right of the farthest right bladder position., it is excluded. Additionally, if the y-axis length of the add region is 1.3 times longer than its x-axis length, it is excluded. If the add-region includes pixels that are too near to the left or too near to the right, it will also be filtered out and not added (within the left or right 15 pixels).

This analysis and selection process completes the first stage of expansion and merging.

Next, we will explain the reasons for filtering each "add region." First, concerning the multiplication of the first step expended image the threshold by 1.5 times the area, it is because, during our analysis, we found that in some cases, certain areas in the images were connected unnecessarily. Upon consultation with medical professionals, we discovered that this connectivity was a result of unnecessary cavities appearing in the ultrasound images. Therefore, after our analysis, we concluded that the original first step expanded image in the bladder area already covers a certain area. Even when

doi:10.6342/NTU202400113

normally connected, an added area should not exceed 1.5 times the original area. If it exceeds this threshold, it likely connects to other cavity areas, so we remove any regions exceeding 1.5 times the area.

Additionally, for "add regions" with an area greater than (image length * image width) / 300 and located more to the right than the farthest right point in the bladder, we don't merge them. This decision is primarily based on the observation that after performing the Exclusive OR operation and adding regions, they are unlikely to have excessively large areas. However, they may still contain small cavities that are not part of the bladder, as described above. In this case, we use relative positioning to determine the location. The preference for the far right point of the bladder is because, in our experimental images, the prostate is typically located in the lower right area. Initially, we attempted to use image analysis to locate the prostate similarly to how we found the basic position of the bladder. However, we found that the prostate, under the mechanism of ultrasound imaging, could sometimes appear as a dark cavity, sometimes not, and sometimes even as a bright anomaly. There was no consistent imaging pattern, so we relied on the relative positioning, specifically to the right of the farthest right point of the original bladder at 0.6 times the threshold. If a region is connected to the bladder, exceeds the area threshold, and its center point is to the right of the farthest right point of the original bladder by a significant margin, we consider it highly likely to be the prostate and exclude it from the expanded bladder region.

Lastly, regarding the y-axis length of "add regions" being more than 1.3 times the x-axis length, this is mainly because the ultrasound images of the bladder that we obtained predominantly exhibit a left-right elongation (where the X-axis is greater than the Y-axis). Even after applying more refined threshold segmentation, this phenomenon

doi:10.6342/NTU202400113

persists. Therefore, when the y-axis length of an "add region" is more than 1.3 times the x-axis length, we consider that what we are adding is likely an unrelated cavity or an image of a region other than the bladder. In such cases, we also remove these regions rather than including them in our analysis.

After explaining the reasons behind each step, let's return to our original method of handling different layers. Essentially, we process three layers. The first layer involves finding the basic position using the first step expanded image, as previously discussed, and then comparing each "add region" to obtain the new bladder. The second layer is built upon the newly merged bladder image obtained in the first layer. We perform the Exclusive OR operation with the results of a 0.8 times threshold and apply bwlabel to obtain various regions. We then individually filter each region to decide whether to include them in the merger. Next, we repeat the same Exclusive OR operation using the results from the 0.8 times threshold, this time compared to the 0.9 times threshold, and apply bwlabel, followed by region selection and merging. This process results in the bladder's expanded contour map for the first stage.

doi:10.6342/NTU202400113

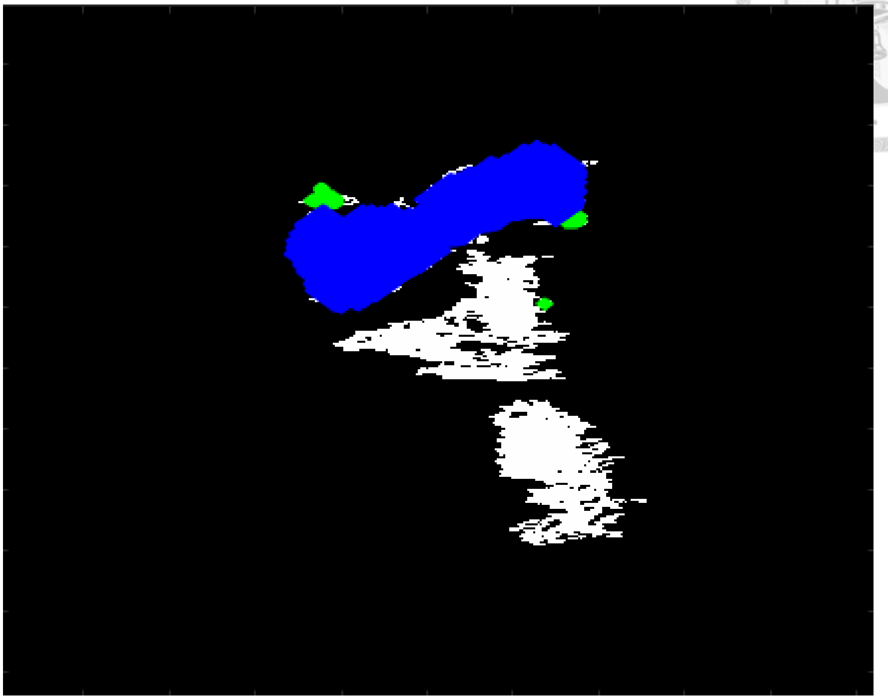

(a)

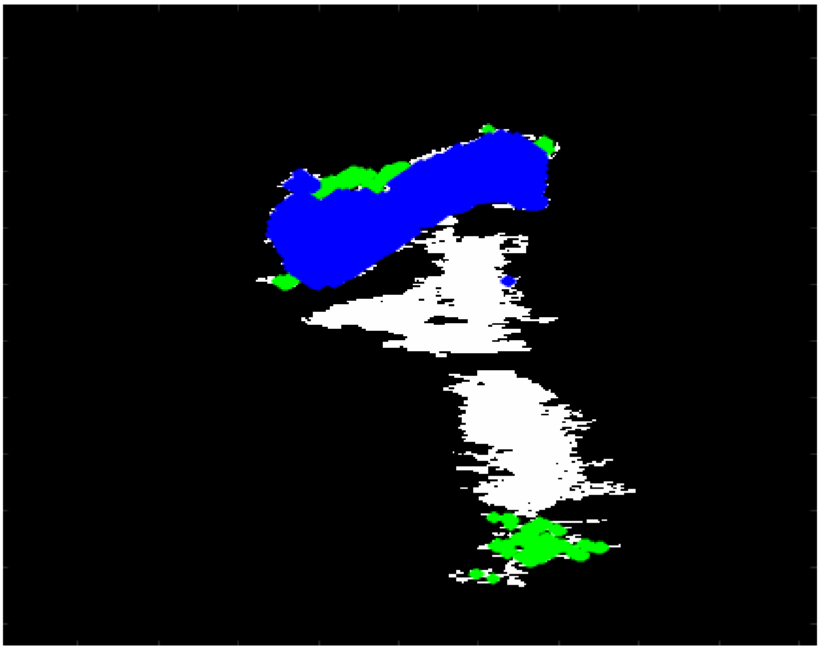

(b)

doi:10.6342/NTU202400113

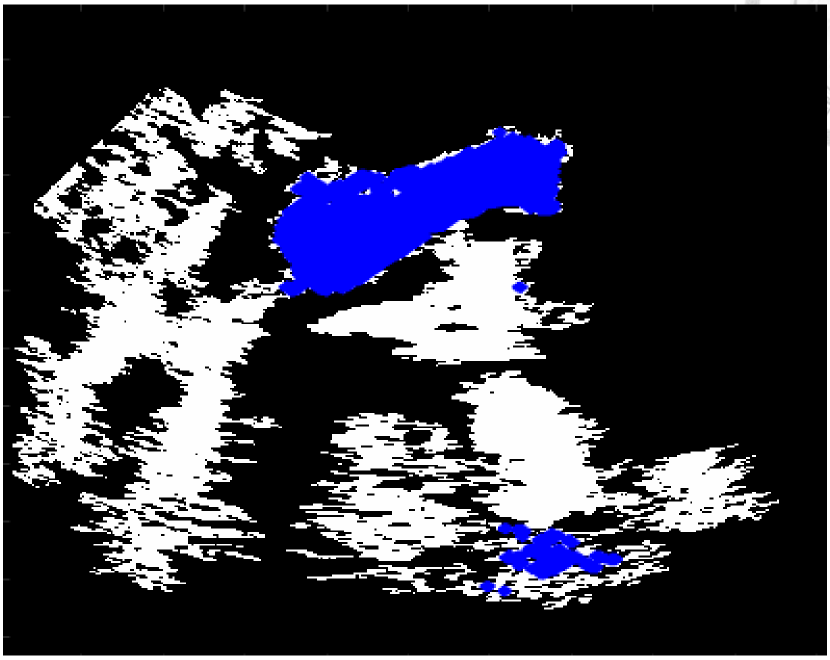

(c)

Fig. 4 8 Examples of Extension. (a): first time extension from 4.3.5 step to 0.6, blue region is original region and green is extension parts. (b): second times extension from 1st step to 0.8, blue region is original region and green is extension part. (c): third times extension from 2st step to 0.9, blue region is original region and green is extension part.

4.3.7 Find Final Bladder Position

After the three expansion steps in the previous second step, we have already obtained most of the bladder's outline. However, at this point, we can observe, as illustrated in the example above, that there are numerous non-bladder regions present in the image. The next step to take is to compare these regions with the smallest bladder

doi:10.6342/NTU202400113

area obtained in the earliest stage, which is the result of 4.3.4, and filter out the true appearance of the bladder.

To do this, we start by applying one opening operation followed by two closing operations to the result mentioned in section 4.3.6. Afterward, we perform region labeling using bwlabel. Then, we scan each region, and if a region contains points from 4.3.4, we include it in the final area. This way, we obtain the final bladder region.

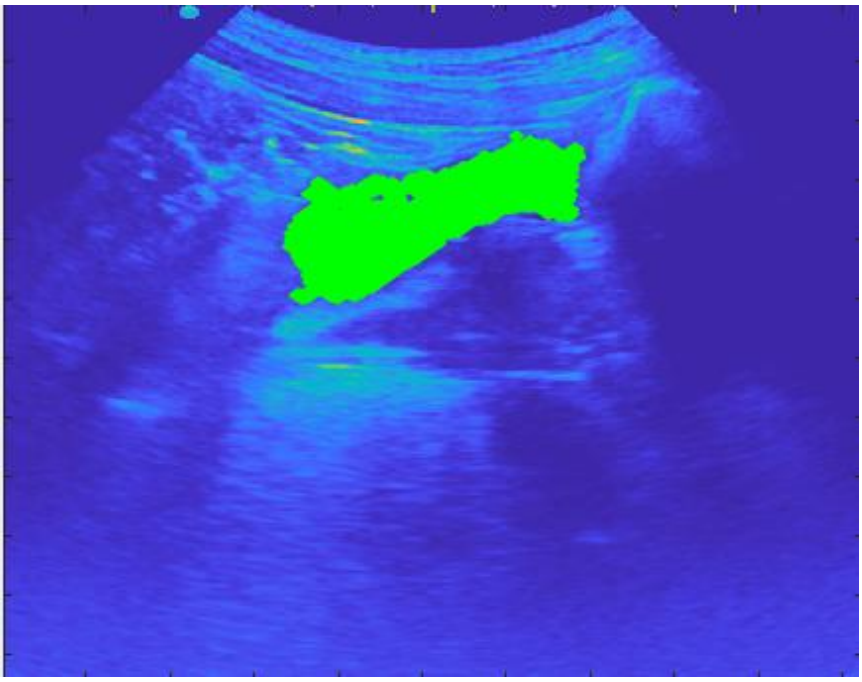

Fig. 4 9 Examples of Final Bladder Outline

4.3.8 Get Bladder Turning Point

Once we have identified the bladder's outline, the next step is to search for the bladder's concave shape to determine the state of IPP (Intravesical Prostatic Protrusion). However, just as mentioned above, the prostate does not exhibit distinct features or characteristics in ultrasound imaging. Sometimes it may have dark areas, sometimes it may be all white, and sometimes it can be noisy and challenging to interpret. We only

doi:10.6342/NTU202400113

know that the prostate is generally located in the lower right corner of the bladder based on discussions with collaborating physicians. In a healthy, non-diseased state, the bladder appears like an elliptical expanding sac under negative pressure. But when there is a prostate condition (IPP), it exhibits a concave shape. So, in this step, we aim to identify and estimate its original healthy state and concave shape to calculate the IPP index. The idea is to use the characteristic of the elliptical expanding sac to make inferences about the health condition.

Therefore, we plan to use the ratio of area to distance and relative positions to infer IPP. First, we use Boundary Descriptors to find the bladder's outer edge, and we calculate a basic value based on the formula as follows.

$$\text{Value} = \frac{\text{Length of Boundary Descriptors}}{\sqrt{area}} \quad (7)$$

According to the formula above, we aim to find the smallest possible value, which means that in theory, we prefer a larger area and shorter connected edges. In other words, we want to find the shortest path, which, in practice, would indicate a concave shape because a concave shape would have a relatively smaller area and relatively longer edges. By finding the shortest path, we aim to identify the bladder's original healthy state.

After introducing the formula and theory, we will provide a detailed explanation of our steps and reasoning.

First, we use the bladder contour we've identified so far and find the rightmost and bottommost points. Because, based on our theory, we assume that the prostate is always located in the lower right part of the bladder, we estimate that we need to search within the area defined by the rightmost point and the bottommost point. Next, we need to

doi:10.6342/NTU202400113

determine whether the Boundary Descriptor selection follows a clockwise or counterclockwise direction. Although the Boundary Descriptor is typically in a clockwise direction, we perform an extra check for safety.

Starting from the rightmost point and moving towards the bottommost point, we calculate the selected path. We use a loop to calculate the direct line between every pair of points and recalculate the new value as follows: $\frac{\text{Length of Boundary Descriptors}}{\sqrt{area}}$. We record the position of the two points that give us the minimum value. It's worth noting that if there is a bladder edge obstruction between two points in a direct line, we don't record that connection. After calculating the minimum path area ratio value for all points, we consider the points where the minimum value occurs as the starting and ending points of the bladder's concave area.

Fig. 4 10 Bladder Turning Point : The light blue area represents the bladder, and the two dark blue asterisks represent the starting and ending points of the concave area.

doi:10.6342/NTU202400113

4.3.9 Estimated Bladder Health Image

After estimating the starting and ending points of the bladder's concave area, the next step is to estimate the bladder's original healthy appearance. Here, we use the elliptical shape mentioned in our discussion with the physician and the labeled samples we have. First, we find the current center point of the bladder and use the previously identified starting and ending points of the concave area. Next, we need to perform a reconstruction by connecting these points. We treat the concave starting and ending points as two points on the ellipse and use the current bladder's center of mass as the center point of the ellipse for calculation. Below is the formula and an illustration of the elliptical calculation: $(x_0,\ y_0)$ is the Center, (x, y) means the Starting and ending points of the elliptical concavity

$$\frac{(x-x_0)^2}{a^2}+\frac{(y-y_0)^2}{b^2}=1 \qquad (8)$$

Convert to the following: $(x_0,\ y_0)$ is the Center, $(x_1,\ y_1)$ is the Starting points of the elliptical concavity, $(x_2,\ y_2)$ is the ending points of the elliptical concavity, a is the Major axis, b is the minor axis.

$$\begin{bmatrix} (x_1-x_0)^2 & (y_1-y_0)^2 \\ (x_2-x_0)^2 & (y_2-y_0)^2 \end{bmatrix} * \begin{bmatrix} \frac{1}{a^2} \\ \frac{1}{b^2} \end{bmatrix} = \begin{bmatrix} 1 \\ 1 \end{bmatrix} \qquad (9)$$

doi:10.6342/NTU202400113

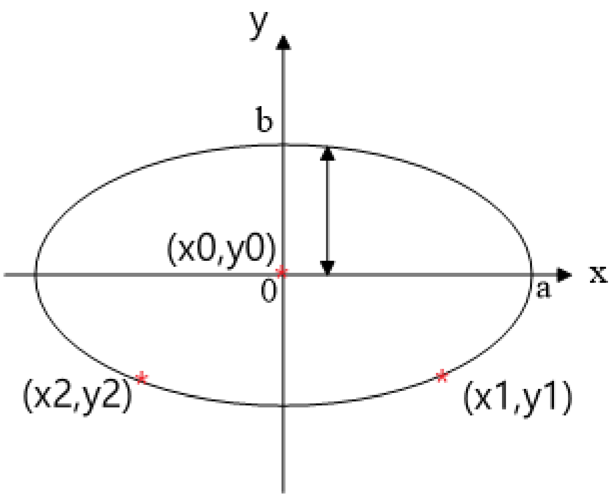

Fig. 4 11 Ellipse

Through the calculations mentioned above, we obtained the connections of the ellipse and implemented them within our bladder region. However, when we compared our calculations with the physician's labels for all our samples, we found that the physician's labels were not always in perfect agreement with the ellipse. Sometimes, the labeled results appeared slightly more flattened compared to the ellipse. To address this, we decided to introduce a weight factor, w. We apply this weight factor w to the elliptical calculations and use (1-w) for the original vertical connection. After conducting tests, we found that a value of w around 0.5 was the most suitable. Therefore, with this weighted calculation, we obtain an estimate of the bladder's original healthy outline.

doi:10.6342/NTU202400113

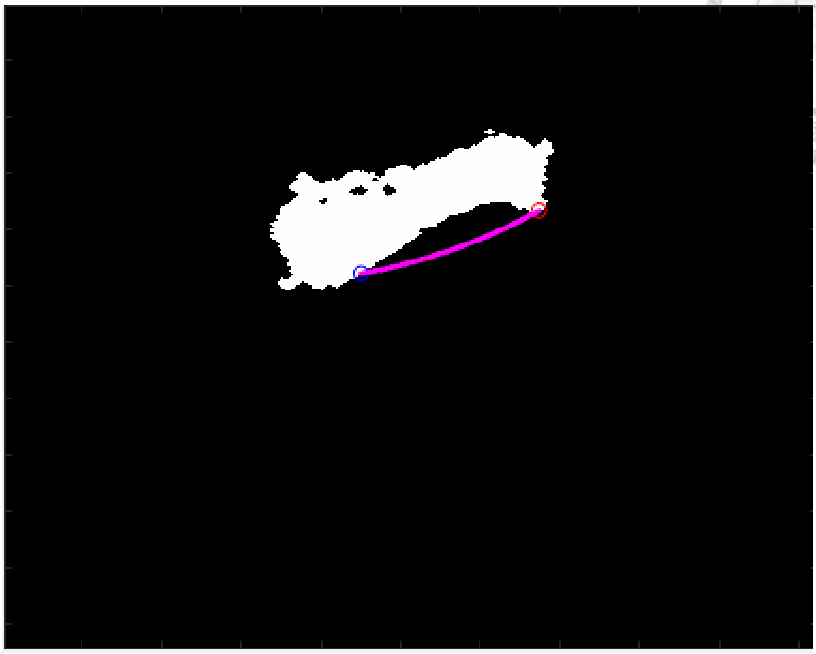

(a)

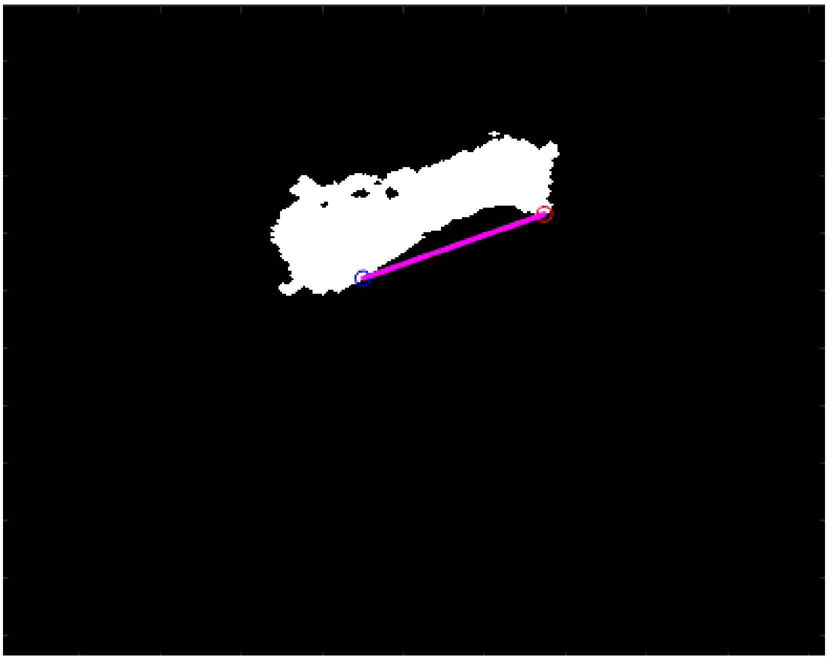

(b)

doi:10.6342/NTU202400113

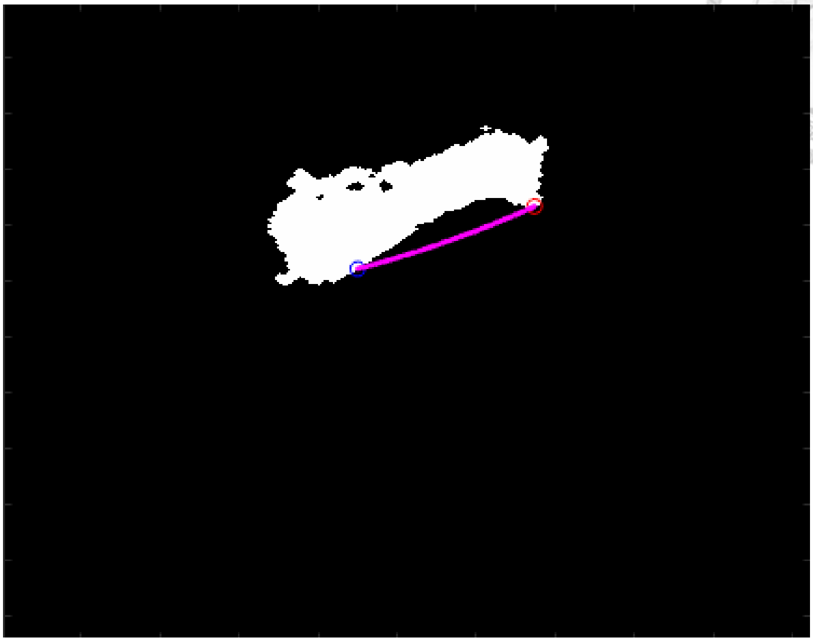

(c)

Fig. 4 12 Examples of estimated bladder in healthy conditions.(a): Link by 1* elliptical curve. (b): Link by 1* straight line. (c): Link by 0.5* elliptical curve and 0.5* straight line.

doi:10.6342/NTU202400113

Chapter 5
Scoring Compare

In a series of processing steps, we identified the bladder contour and bladder area from bladder ultrasound. Subsequently, we assessed the bladder's health status. However, after a series of processing steps, we have not yet performed an actual numerical analysis and comparative table. Therefore, in this section, we will explain.

5.1 Physician's marking calculation

The bladder ultrasound image and the marked lines provided by the physician are on separate images. Therefore, we need to merge the two images. Additionally, since the markings are not quantified, we need to process the physician's markings to make them quantifiable. First, we identify the two intersection points of the circled lines for the bladder and prostate positions marked by the physician. Only after this can we proceed with numerical scoring. The method of numerical scoring will be explained later. Our main focus here is to display the physician's marked image, merge it with the ultrasound image, and identify the intersection points.

doi:10.6342/NTU202400113

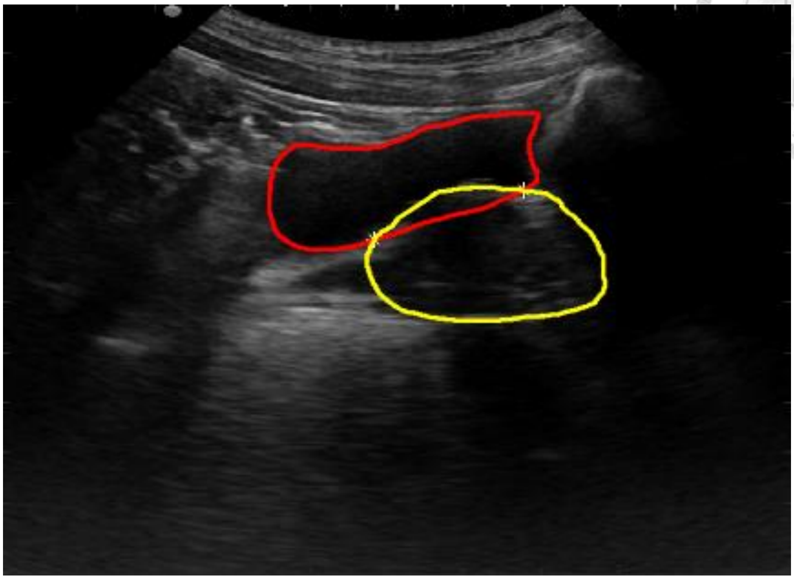

Fig. 5 1 Physician's marking calculation

5.2 Midpoint vertical distance

This is a common method for measuring the IPP in the medical field, as inquired by our collaborating physician. The approach involves identifying the intersection points at the depression of the bladder, connecting two points, and then measuring the vertical distance from the midpoint to the concave region inside the bladder. If we are using the physician's annotated image, we take the intersection points of the two annotated circles to calculate the vertical distance. If we have identified the bladder contour ourselves, we can connect the two intersection points from Chapter Four and measure the vertical distance from the midpoint to the inner concave region of the bladder.

doi:10.6342/NTU202400113

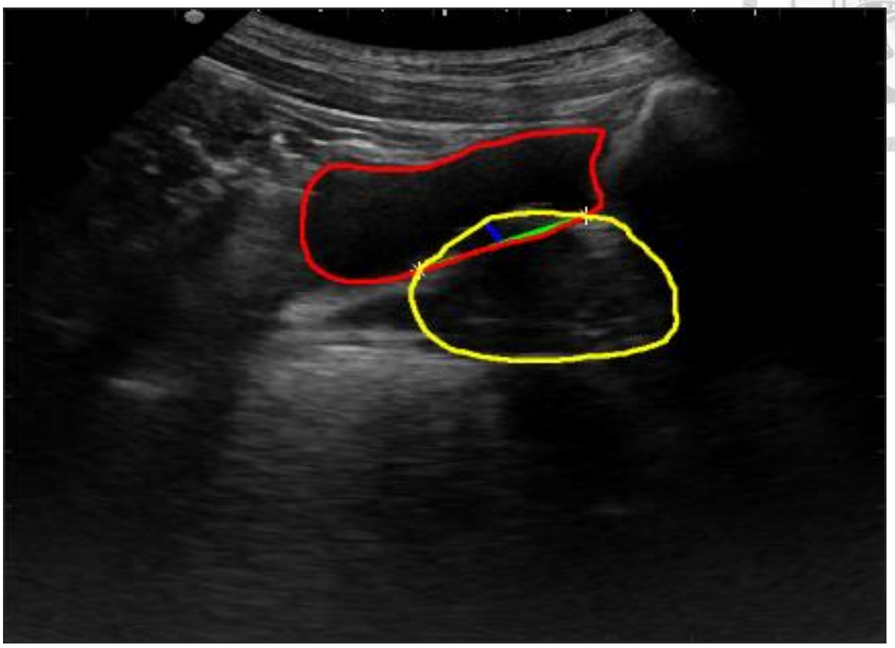

(a)

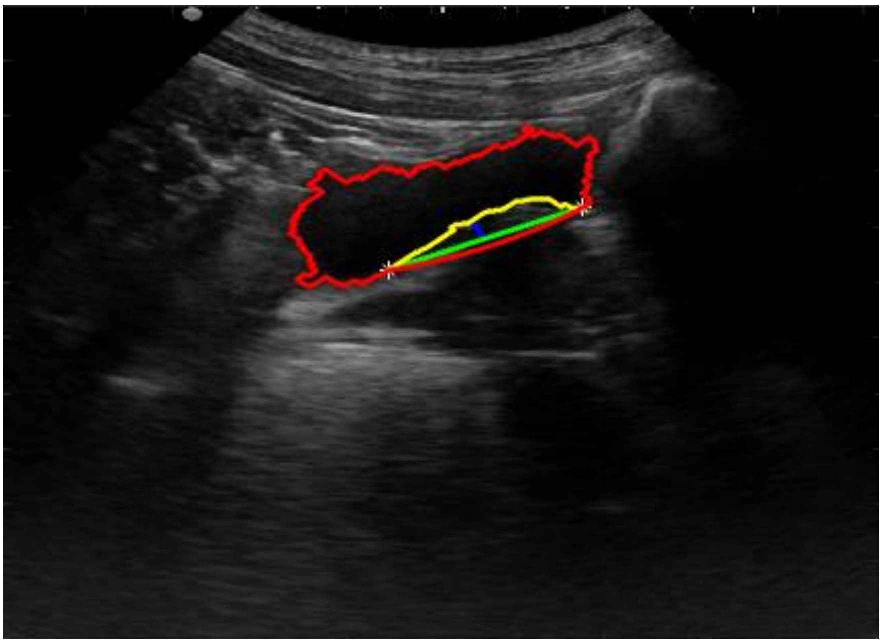

(b)

Fig. 5 2 Comparison of Actual Results in IPP: (a): Physician's marking . (b):

doi:10.6342/NTU202400113

Experimental results The red line represents the bladder, the yellow line represents the prostate, white asterisks denote the intersection points of the two, the green line signifies the connection between the intersection points, and the blue line represents the IPP distance.

5.3 Ellipse PCA distance

From the above method, we can identify the common IPP measurement used by physicians in the medical field. However, using this method alone, we cannot estimate the original contour of a healthy bladder. To assess the accuracy of our reconstruction, we introduced an additional method to estimate the bladder. In this case, we utilized the Elliptical Estimation using Principal Component Analysis (PCA). The principle behind this approach is based on the inference that the bladder and prostate, in a healthy state, should exhibit an elliptical or sac-like ultrasound shape. Therefore, we applied PCA to estimate the bladder by assuming that the intersection point is approximately elliptical. We conducted a horizontal projection to calculate the major and minor axes of the ellipse. We used the minor axis of the ellipse as a comparative measurement standard to evaluate how accurately we reconstructed the appearance of a healthy bladder. It is important to note that these results are unrelated to the IPP index; they serve solely as an indicator for the degree of accuracy in estimating the appearance of a healthy bladder.

Here, we provide a detailed explanation of the PCA methodology, which is similar to the approach described in Section 4.3.9 when estimating the appearance of the kidney using elliptical estimation. Firstly, we utilize the previously estimated healthy bladder

doi:10.6342/NTU202400113

and identify its intersection line with the kidney. The region of intersection between these two serves as the target for our processing. The following is our formula:

(x_0,y_0) is the centroid, (x_n, y_n) are any point within the range

$$z = [(x_n-x_0),(y_n-y_0)], \quad z_1 = z^T * z \tag{10}$$

[E,D] : matrix D is eigenvalues, and matrix E whose columns are the corresponding right eigenvectors of z_1

x_1 = z * (first column vector of E), x_2 = z * (second column vector of E);

$T_1 = E(|x_1|)$, $T_2 = E(|x_2|)$, E( ) represents taking the average

$$\begin{cases} a_1 = \frac{3\pi}{4} * T_{1,1} \quad , \quad a_2 = \sqrt{4 * T_{2,1}} \\ b_1 = \frac{3\pi}{4} * T_{1,2} \quad , \quad b_2 = \sqrt{4 * T_{2,2}} \end{cases} \tag{11}$$

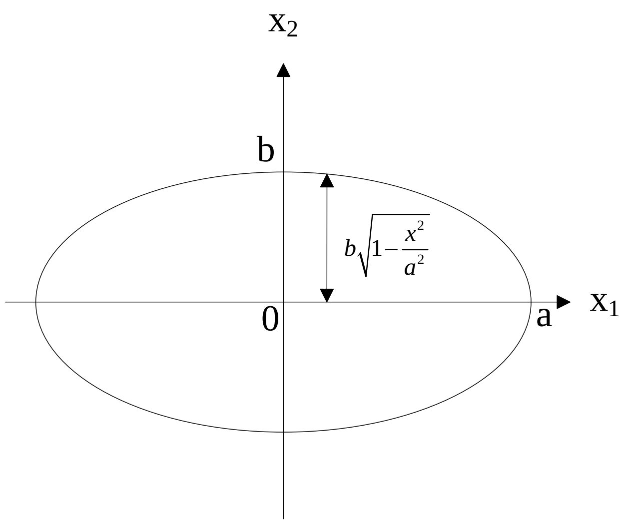

After the PCA calculation mentioned above, we obtain the major and minor axes (a,

doi:10.6342/NTU202400113

b) of the ellipse. We then use the minor axis b as the standard for reconstructing a healthy bladder.

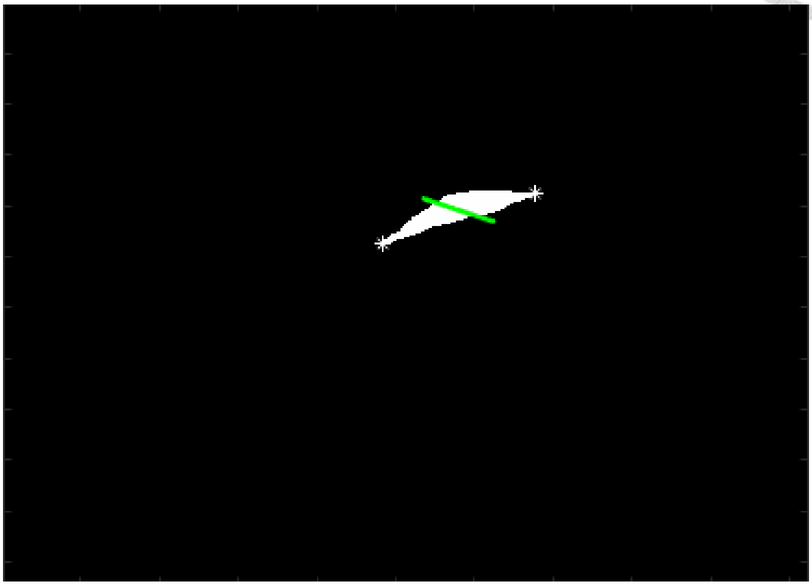

(a)

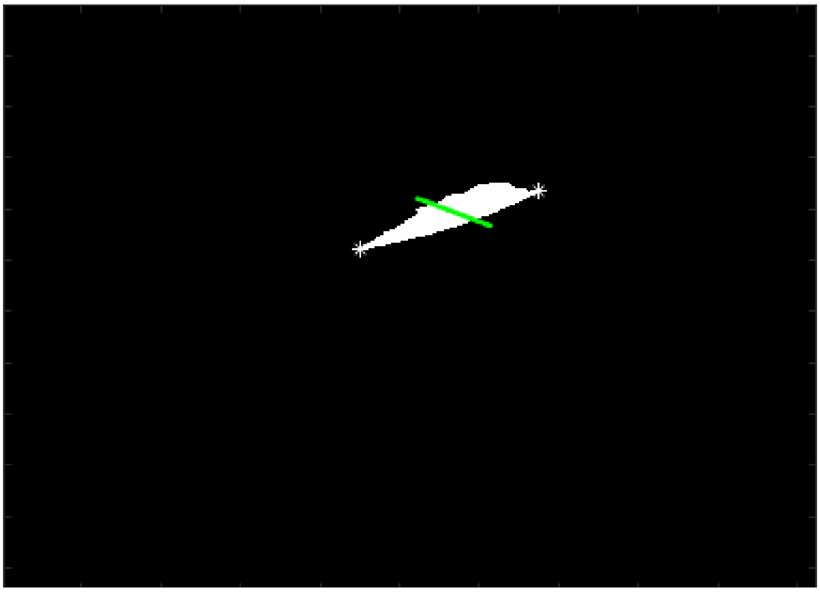

(b)

Fig. 5 3 PCA distance: (a): PCA in Physician's marking. (b): PCA in my result

doi:10.6342/NTU202400113

5.4 Unit Conversion

While the above method allows us to explicitly obtain the calculated depth of the bladder depression and the depth of the physician's marked range, a crucial aspect is determining whether there is a need for treatment related to the IPP. The key criterion for assessing IPP is whether it reaches 5.5 millimeters. Therefore, we need to perform unit conversion to transform the original pixel values into millimeters. We adopted a method using the conversion between millimeters and pixels based on marked points on the image. Starting from the highest point at mark 1 to the lowest point at mark 5, we performed calculations and found a total of 180 pixels. Upon meticulous examination, we confirmed that each interval had a consistent number of pixels. Therefore, we inferred that in our experimental ultrasound images, each millimeter corresponds to 36 pixels. Using this conversion factor as a basis, we recalculated our previous results and made the final comparisons

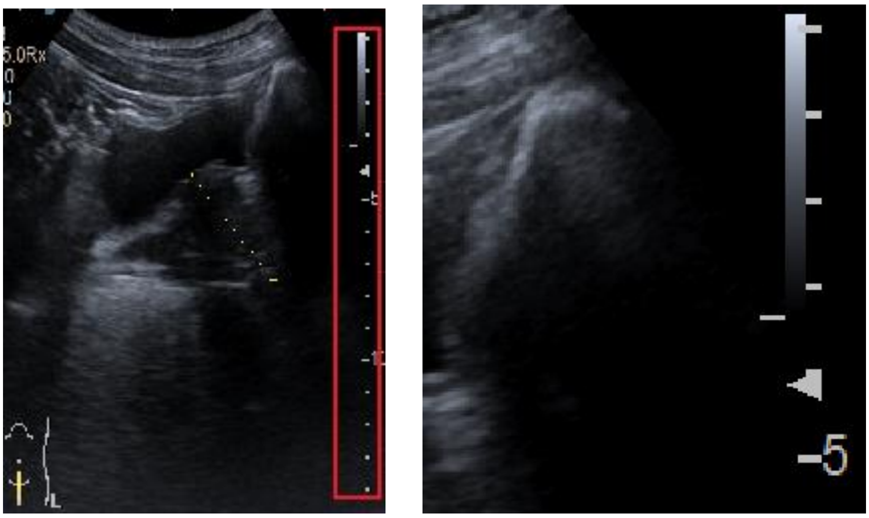

(a) (b)

Fig. 5 4 Unit Conversion Image: (a): part of the ultrasound image the red box indicates the position of the calibration ruler. (b): magnified ultrasound.

doi:10.6342/NTU202400113

5.5 Result Compare

For the comparison of results, we primarily divide it into two parts. The first part involves calculating the accuracy of correctly identifying the IPP for processing. Considering a 10% margin of error, so we discussed with the physician to set 5 millimeters as the threshold for severe processing. The second part involves comparing the depression values of IPP, focusing on targets where IPP is greater than 5 millimeters.

Table 5. 5 Results and error comparison table

IMAGE NUM	LABEL	RESULT	ATTENTION	ERROR(%)
1-1	6.7	5.3	V	20.89
1-2	8.33	8.33	V	0
1-3	0.28	0.28	X	
1-4	0.56	0.56	X	
1-5	9.17	6.94	V	24.32
2-1	4.4	5.8	T	31.81
2-2	8.89	6.11	V	31.27
2-3	6.94	6.38	V	8.07
2-4	0.28	1.67	X	
2-5	5.83	5	V	14.24
2-6	0.28	2.22	X	
2-7	0.28	1.67	X	
2-8	13.3	13.3	X	0

doi:10.6342/NTU202400113

2-9	1.39	2.78	X	
2-10	0.28	0.83	X	
2-11	5	6.11	V	22.2
2-12	0.28	1.94	X	
2-13	18.6	25.3	V	36.02
2-14	0.28	0.28	X	
2-15	3.06	3.06	X	
2-16	5.56	5.56	V	0
2-17	3.33	3.33	X	
2-18	0.28	3.33	X	
2-19	12.8	11.7	V	8.59
2-20	0.28	1.11	X	

We would like to provide a detailed explanation of the comparison table mentioned above. The images are categorized based on the batches provided by the physician, namely the first batch and the second batch. The units for both marking and result comparison are in millimeters, rounded to the second decimal place. The error percentage is calculated only for targets where IPP is greater than 5 millimeters, and it is also rounded to the second decimal place. The calculation formula is as follows: (Label Value – Result Value) / Label Value

Based on the above results, we summarize the data, presenting a 95% accuracy rate in predicting the need for further examination of bladder difficulty. In the second step, when predicting depression greater than 5 millimeters, requiring an advanced examination of bladder IPP depression, we achieve an average accuracy of 16.45%

doi:10.6342/NTU202400113

5.6 Error attribution

Regarding the reasons for errors, we have a few findings. First, the data we received is manually annotated, and the values are subject to human observation. In some scenarios, we noticed that when we zoomed in on the images, many annotations might have some human observation errors, possibly due to the distance between the markings and the edges of the bladder image. The second potential source of error comes from using the area-to-perimeter ratio to find the shortest distance. This distance may not precisely represent the actual intersection point. The most common occurrence is when the starting and ending points of the intersection between the bladder and prostate form an 'M' shape in the depression, and it should connect from the far right to the far left initially. However, we might have identified only the midpoint connecting to the far left to select as the starting point. Although the proportion of this occurrence is not high, we have observed some instances of this condition. The third potential reason is incomplete identification of the bladder contour, possibly due to the bladder being connected to other cavities or issues during the imaging procedure. This insufficient completeness in contour identification might result in errors in our analysis. However, instances of this situation are also relatively rare.

doi:10.6342/NTU202400113

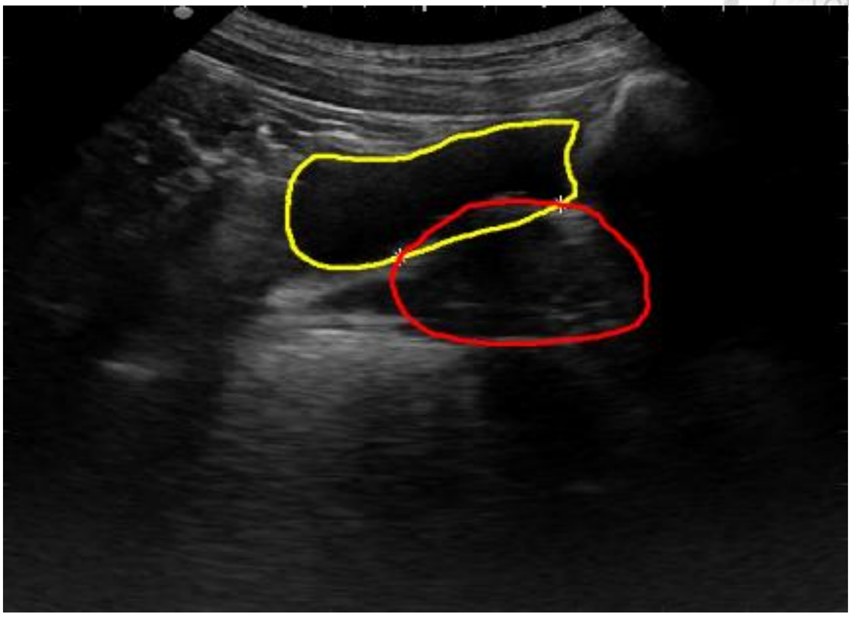

(a)

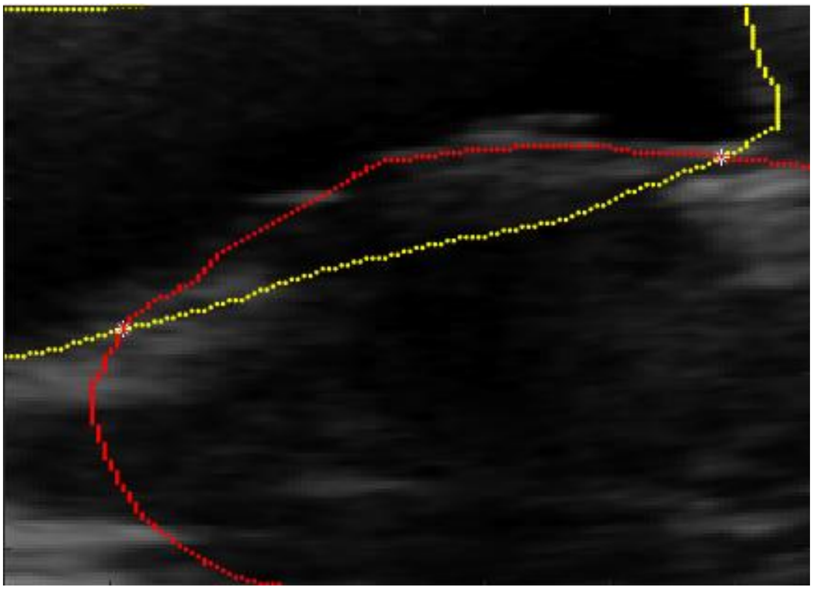

(b)

doi:10.6342/NTU202400113

(c)

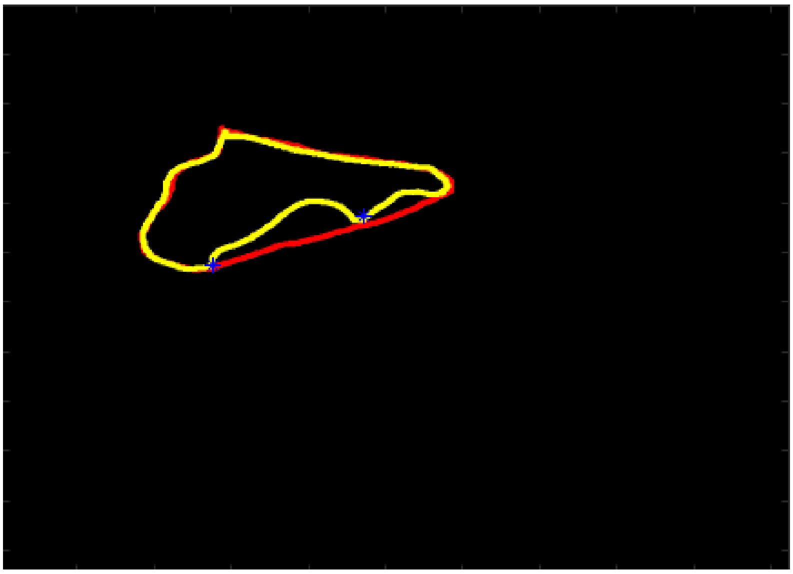

(d)

doi:10.6342/NTU202400113

(e)

Fig. 5 5 Error attribution Reason: (a) & (b) provide a comparison with the physician's annotations. When viewed at normal size, they may appear to be marked on the edge of the bladder. However, upon closer inspection of the enlarged results of (b), it becomes evident that there is some distance from the bladder edge. (c) & (d) provide a comparison in a scenario with a bladder depression resembling an 'M' shape. There is a discrepancy in the determined points between the physician's marking in (c) and our results in (d). (e) illustrates that in some cases, our results may show a slight distance between the starting and ending points of the bladder depression. The blue asterisks represent the physician's markings, while the green asterisks represent our marked results, indicating a minor discrepancy.

doi:10.6342/NTU202400113

Chapter 6
Experimental Results

Since our paper primarily focuses on medical images of bladder ultrasound, although we have discussed the numerical results in the previous sections, our findings, aside from being quantified, can also be utilized to facilitate rapid image interpretation by physicians. To illustrate these points, we present ten processed results in this paper. In each pair of images, the left part shows the results annotated by the physician, while the right part displays our processed results. The yellow line represents the expected appearance of the bladder in healthy conditions, and the red line indicates the condition where the prostate causes depression in the bladder.

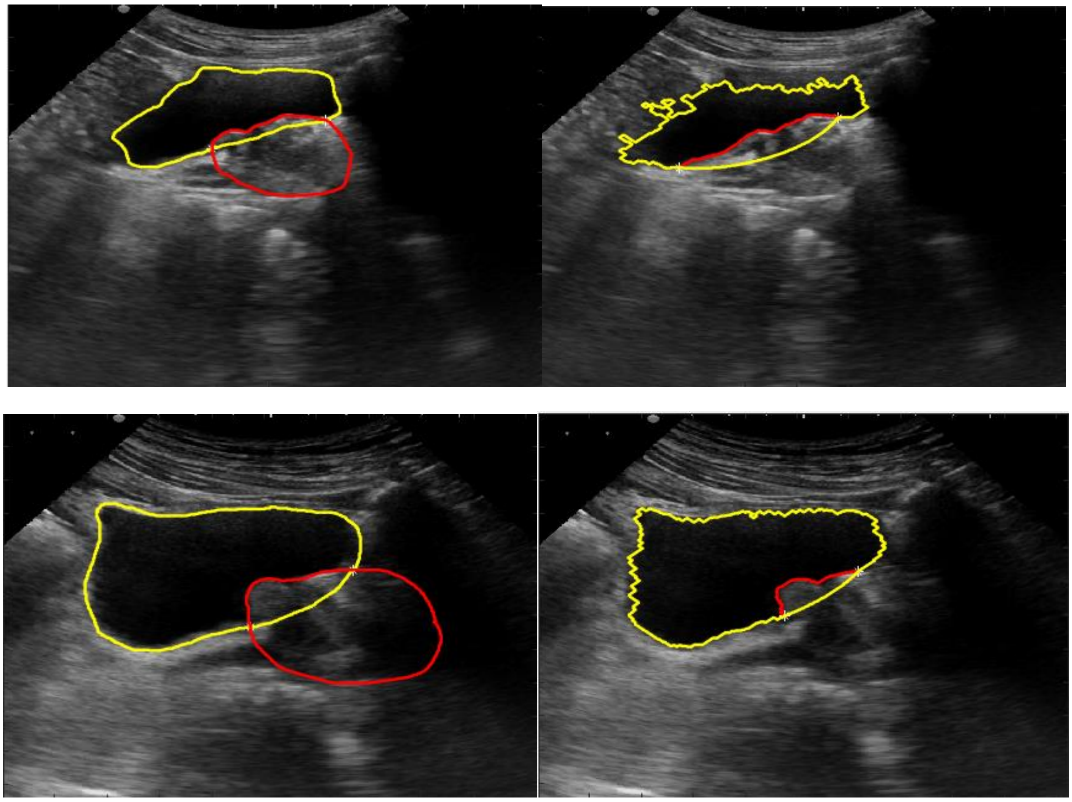

doi:10.6342/NTU202400113

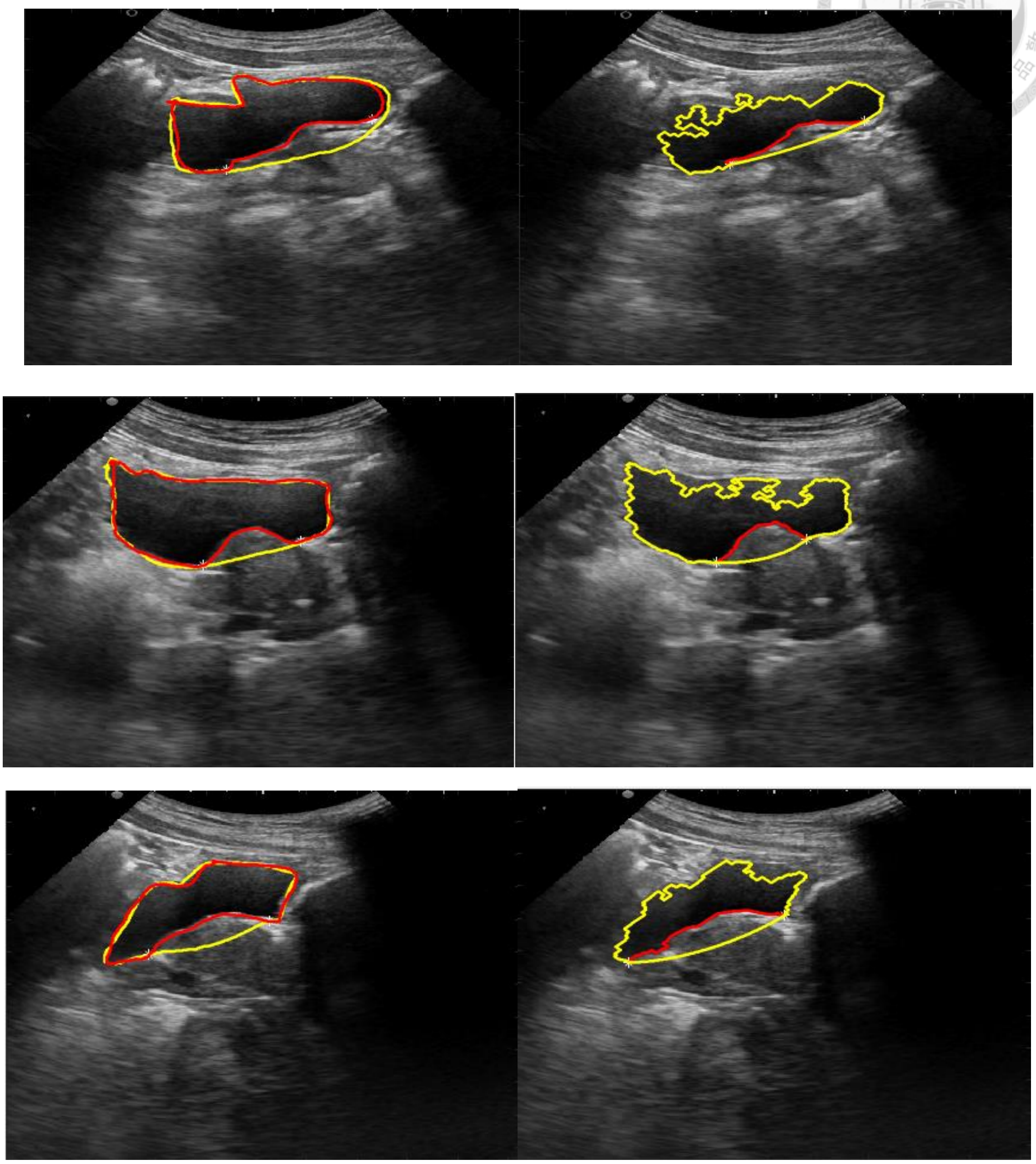

doi:10.6342/NTU202400113

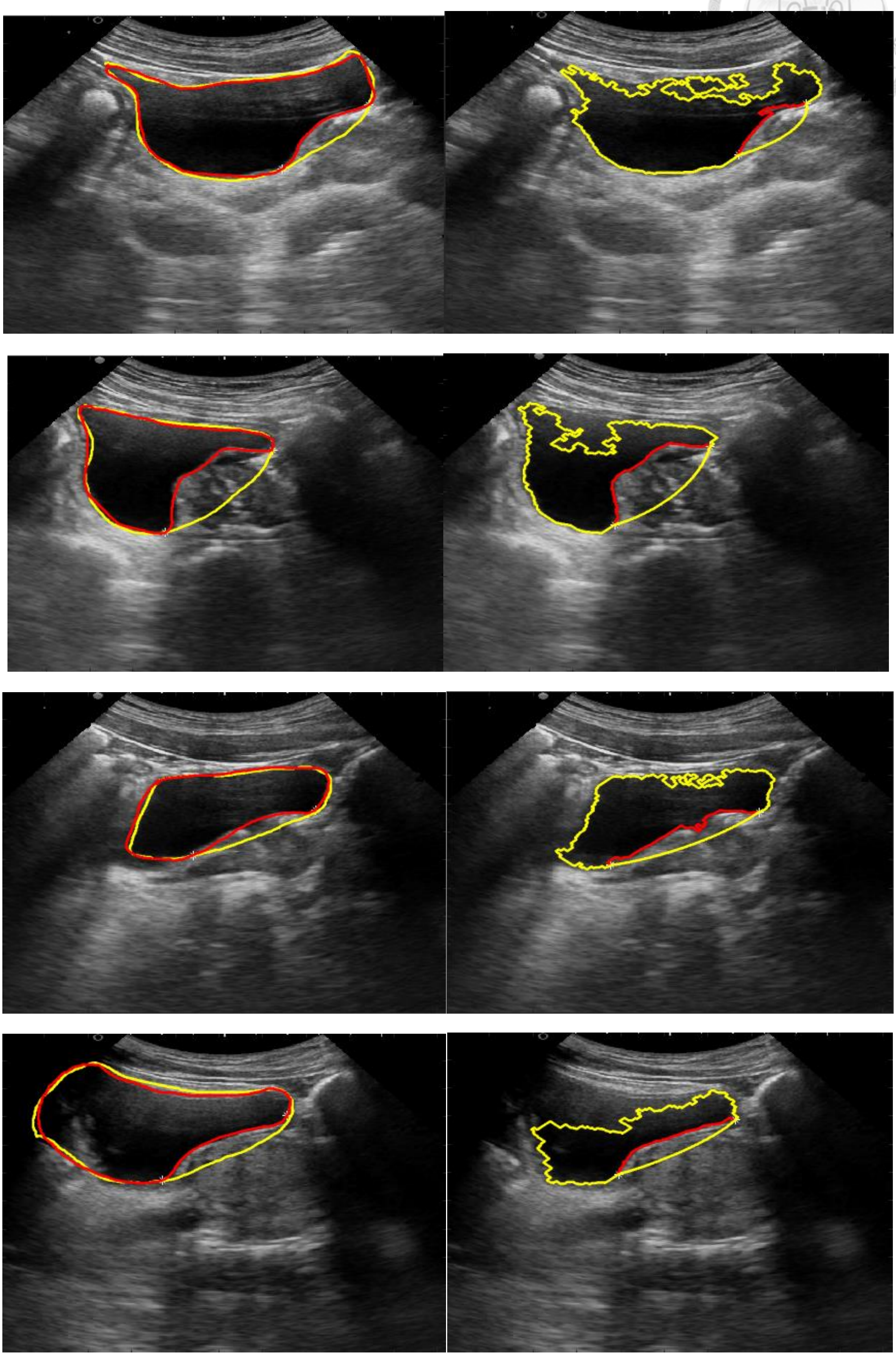

doi:10.6342/NTU202400113

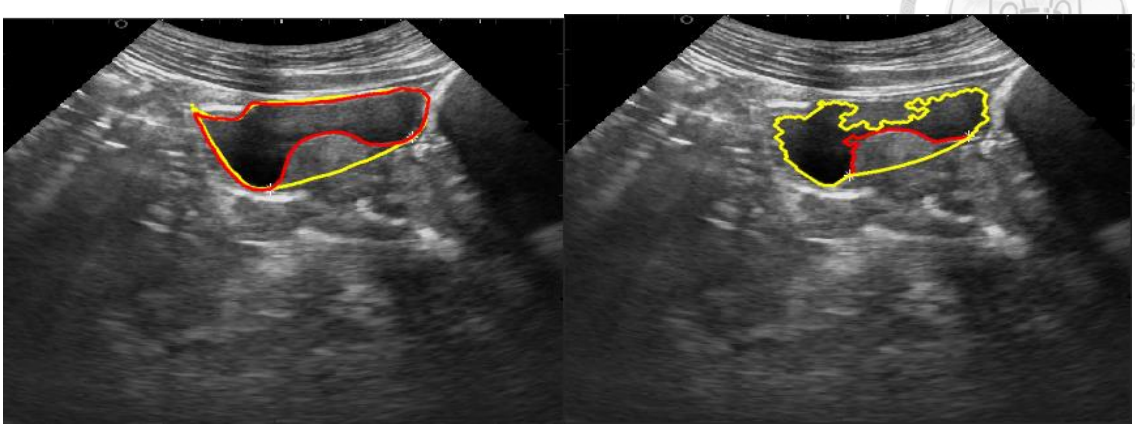

Fig. 6 1 Images result compare

doi:10.6342/NTU202400113

Chapter 7
Conclusion

The detailed research primarily focuses on the concavity index of the bladder and the interpretation of prostate protrusion into the bladder. The identification methods mainly employed include noise reduction, edge detection, dynamic thresholding, morphology, and the shortest distance evaluation for processing. Measurement standards are established using PCA distance measurements and vertical distance from the central point.

The algorithm we developed for processing bladder ultrasound images (IPP):

1. The initial step involves handling non-image data related to patient records.

2. Subsequent steps entail the removal of noise from ultrasound images.

3. The primary location of the bladder is determined by comparing it with the primary brightness threshold.

4. The prostate's position is deduced by iteratively enhancing the appearance of the bladder relative to brightness.

5. Non-bladder sections are removed based on relative position and morphological analysis.

6. By comparing the boundary Descriptor's perimeter and area ratio tables, we identify the estimated junction point of the bladder-prostate depression.

7. Using the previously mentioned processed image, the extent of bladder concavity is estimated through vertical projection and the PCA algorithm.

Based on the methods above, the concavity disease index of bladder ultrasound

doi:10.6342/NTU202400113

images can be determined.

Reference

[1] Rafael C. Gonzalez • Richard E. Woods "Digital Image Processing" 4E, pp. 328-332

[2] Peixuan Zhang & Fang Li(2014)" A New Adaptive Weighted Mean Filter for Removing Salt-and-Pepper Noise" IEEE Signal Processing Letters. pp.1280 - 1283

[3] Ian T. Young& Lucas J. van Vliet (1995) " Recursive implementation of the Gaussian filter " Signal Processing. pp.139-151

[4] G. Deng & L.W. Cahill (1993)"An adaptive Gaussian filter for noise reduction and edge detection".

[5] https://zh.wikipedia.org/wiki/%E9%AB%98%E6%96%AF%E6%BF%BE%E6%B3%A2%E5%99%A8

[6] Johannes P.F. D'Haeyer "Gaussian Filtering of Images: A Regularization Approach." Signal Processing, pp. 169-181.

[7] http://www.faadooengineers.com/online-study/post/ece/digital-image-processing/1129/boundary-descriptors

[8] Meyer, F., & Beucher, S. "Morphological segmentation." Journal of Visual Communication and Image Representation, 1990.

[9] Bhutada, S., Yashwanth, N., Dheeraj, P., & Shekar, K. . "Opening and closing in morphological image processing." World Journal of Advanced Research and Reviews, 2022.

[10] Khairul Anuar Mat Said*, Asral Bahari Jambek*and Nasri Sulaiman (2016)"A study of image processing using morpholoical opening and closing processes " International Journal of Control Theory and Applications pp.15-21

[11] C. Ronse & H.J.A.M. Heijmans "The algebraic basis of mathematical morphology: II. Openings and closings" CVGIP: Image Understanding pp.74-97

doi:10.6342/NTU202400113

[12] https://jason-chen-1992.weebly.com/home/-morphology

[13] https://medium.com/%E9%9B%BB%E8%85%A6%E8%A6%96%E8%A6%BA/%E5%BD%A2%E6%85%8B%E5%AD%B8-morphology-%E6%87%89%E7%94%A8-3a3c03b33e2b

[14] Szabo, T. L. (2014). "Diagnostic Ultrasound Imaging: Inside Out." pp. 1-37

[15] Rumack, C. M., & Levine, D. (2017). "Diagnostic Ultrasound, 2-Volume Set" (5th ed.). August 8, 2017.

[16] https://www.uscultrasound.com/what-is-ultrasound-and-how-does-it-work/

[17] Andersson KE & Arner A.(2004) "Urinary bladder contraction and relaxation: physiology and pathophysiology." PP.935-986

[18] Banker, Hiral, and Selvarajan, Santosh K. "Prostate Imaging."

[19] Z, Keqin, X, Zhishun, Z, Jing, W, Haixin, Z, Dongqing, & S, Benkang.(2007) "Clinical significance of intravesical prostatic protrusion in patients with benign prostatic enlargement." pp.1096-1099.

[20] Su Hwan Shin, Jong Wook Kim, Jin Wook Kim, Mi Mi Oh, Du Geon Moon. "Defining the Degree of Intravesical Prostatic Protrusion in Association With Bladder Outlet Obstruction" Department of Urology, Korea University Guro Hospital, Seoul, Korea.

[21] Lee, C. H., & Ha, H. K. (2014). "Intravesical prostatic protrusion as a predictor of early urinary continence recovery after laparoscopic radical prostatectomy. "International Journal of Urology pp.653-656.

[22] https://commons.wikimedia.org/wiki/File:Prostate.jpg

doi:10.6342/NTU202400113